Article
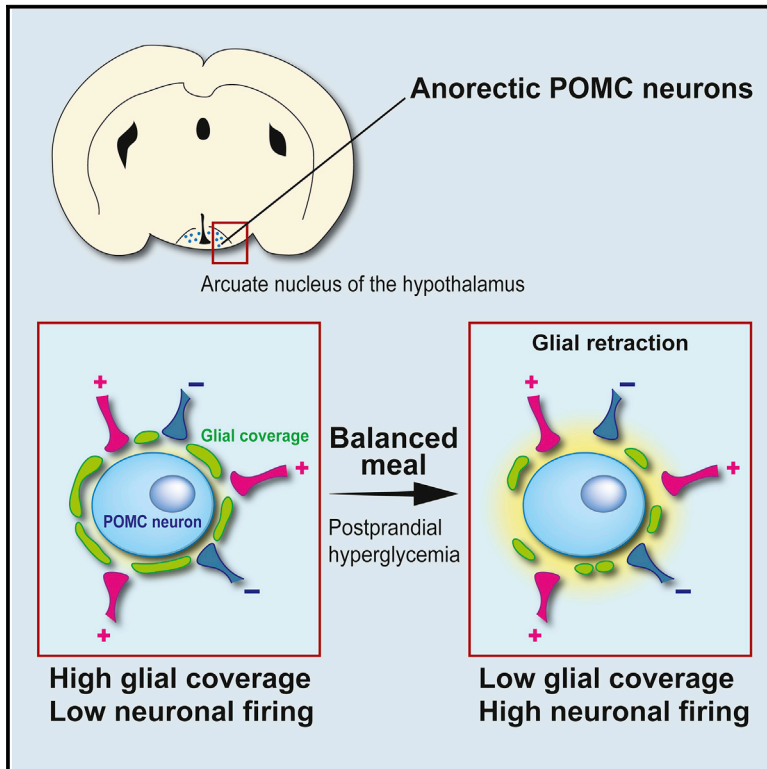
Postprandial Hyperglycemia Stimulates Neuroglial Plasticity in Hypothalamic POMC Neurons after a Balanced Meal

Graphical Abstract

Highlights

- Postprandial hyperactivity of hypothalamic POMC neurons involves synaptic plasticity

- Postprandial plasticity of POMC neurons engages glial retraction

- Postprandial glial retraction around POMC neurons is triggered by hyperglycemia

- Glial retraction on POMC neurons modifies meal pattern

Authors

Danaé Nuzzaci, Céline Cansell, Fabienne Liénard, ..., Jean-Louis Nahon, Carole Rovère, Alexandre Benani

Correspondence

alexandre.benani@u-bourgogne.fr

In Brief

State-dependent plasticity in neuronal circuits controlling hunger is well established. Nuzzaci et al. show that this process is recapitulated after a meal. Postprandial hyperglycemia induces glial retraction around hypothalamic POMC neurons, which increases the activity of these anorectic neurons. This macronutrient-dependent plasticity provides a neurobiological basis for satiety.

CellPress

Postprandial Hyperglycemia Stimulates Neuroglial Plasticity in Hypothalamic POMC Neurons after a Balanced Meal

Danaé Nuzzaci,[1,9] Céline Cansell,[2,9] Fabienne Liénard,[1] Emmanuelle Nédélec,[1] Selma Ben Fradj,[1] Julien Castel,[3] Ewout Foppen,[3] Raphael Denis,[3] Dominique Grouselle,[4] Amélie Laderrière,[1] Aleth Lemoine,[1] Alexia Mathou,[1] Virginie Tolle,[4] Tony Heurtaux,[5] Xavier Fioramonti,[6] Etienne Audinat,[7] Luc Pénicaud,[8] Jean-Louis Nahon,[2] Carole Rovère,[2] and Alexandre Benani[1,10,*]

[1]Centre des Sciences du Goût et de l'Alimentation, AgroSup Dijon, CNRS, INRAE, Université Bourgogne Franche-Comté, 21000 Dijon, France
[2]Université Côte d'Azur, CNRS, Institut de Pharmacologie Moléculaire et Cellulaire, 06560 Valbonne, France
[3]Unité "Biologie Fonctionnelle & Adaptative," CNRS, Université Paris Diderot, 75005 Paris, France
[4]Université de Paris, Institute of Psychiatry and Neuroscience of Paris (IPNP), INSERM U1266, 75014 Paris, France
[5]Luxembourg Center of Neuropathology, Department of Life Sciences and Medicine, University of Luxembourg, 4362 Esch-sur-Alzette, Luxembourg
[6]Laboratoire NutriNeuro, INRA, Université de Bordeaux, 33076 Bordeaux, France
[7]Institut de Génomique Fonctionnelle, Université de Montpellier, CNRS, INSERM, 34094 Montpellier, France
[8]StromaLab, CNRS, EFS, INP-ENVT, INSERM, Université Paul Sabatier, 31100 Toulouse, France
[9]These authors contributed equally
[10]Lead Contact
*Correspondence: alexandre.benani@u-bourgogne.fr
https://doi.org/10.1016/j.celrep.2020.02.029

SUMMARY

Mechanistic studies in rodents evidenced synaptic remodeling in neuronal circuits that control food intake. However, the physiological relevance of this process is not well defined. Here, we show that the firing activity of anorexigenic POMC neurons located in the hypothalamus is increased after a standard meal. Postprandial hyperactivity of POMC neurons relies on synaptic plasticity that engages pre-synaptic mechanisms, which does not involve structural remodeling of synapses but retraction of glial coverage. These functional and morphological neuroglial changes are triggered by postprandial hyperglycemia. Chemogenetically induced glial retraction on POMC neurons is sufficient to increase POMC activity and modify meal patterns. These findings indicate that synaptic plasticity within the melanocortin system happens at the timescale of meals and likely contributes to short-term control of food intake. Interestingly, these effects are lost with a high-fat meal, suggesting that neuroglial plasticity of POMC neurons is involved in the satietogenic properties of foods.

INTRODUCTION

Obesity is a worldwide epidemic that poses major risks for diabetes, cardiovascular diseases, and certain forms of cancer. Over the past years, genome-wide scans in human subjects have mapped several loci on chromosomes for body mass index (BMI). Identified genes in BMI-associated loci are enriched in the brain and mainly related to neurodevelopment and neuronal biology, providing support for a crucial role of the central nervous system in obesity susceptibility (Hoffmann et al., 2018; Locke et al., 2015; Willer et al., 2009). In particular, glutamatergic neurotransmission and synaptic plasticity have emerged as two major pathways implicated in the regulation of body weight (Locke et al., 2015). Fundamental studies carried out on rodents clearly evidenced synaptic plasticity in neuronal circuits controlling appetite and metabolism (Cristino et al., 2013; Horvath and Gao, 2005; Labouèbe et al., 2013; Lim et al., 2012; Pinto et al., 2004; Wang et al., 2016). For instance, synaptic connections in the melanocortin system, a master regulator of energy balance, are significantly reorganized during starvation (Kong et al., 2016; Liu et al., 2012; Vong et al., 2011; Yang et al., 2011) or overfeeding (Benani et al., 2012).

The balance between excitatory and inhibitory inputs on the two antagonistic components of the melanocortin system, anorexigenic pro-opiomelanocortin (POMC) and orexigenic agouti related peptide (AgRP) neurons, varies according to energy availability and related changes in blood hormones. Remarkably, hormones coordinate synaptic remodeling in a coherent manner with the behavioral effect. Furthermore, brain-targeted manipulation of plasticity-related molecules impairs a number of homeostatic responses following disruption of energy balance and makes mice prone to obesity (Benani et al., 2012; Brenachot et al., 2014, 2017; Rathjen et al., 2017). Therefore, synaptic plasticity of the melanocortin system is viewed as an adaptive response aimed at preserving energy homeostasis (Dietrich and Horvath, 2013; Zeltser et al., 2012). Nevertheless, the physiological relevance of this mechanism is still unclear. To date, synaptic remodeling in the melanocortin system has been described in response to large,

supraphysiological changes in blood hormone concentrations caused by drastic metabolic challenges (Benani et al., 2012; Liu et al., 2012; Vong et al., 2011; Yang et al., 2011) or by hormone replacement therapy in experimental models (Gao et al., 2007; Gyengesi et al., 2010; Pinto et al., 2004). Thus, it is still unknown whether synaptic plasticity in brain feeding circuits is triggered upon extreme metabolic conditions only or whether it is also recapitulated at the timescale of meals in response to subtle metabolic changes. Answering this issue is crucial to define the value of plasticity of brain feeding circuits.

Interestingly, application of recombinant hormones on brain slices can alter the synaptic strength between neurons involved in regulation of feeding in less than 1 h (Labouèbe et al., 2013; Vong et al., 2011; Yang et al., 2011). This timescale fits with the kinetic of release of ingestion-related cues and is consistent with control of satiety by synaptic plasticity processes. POMC neurons located in the arcuate nucleus of the hypothalamus are nutritionally regulated (Beutler et al., 2017; Chen et al., 2015; Mandelblat-Cerf et al., 2015; Vong et al., 2011; Yang et al., 2011) and involved in control of satiety (Aponte et al., 2011; Atasoy et al., 2012; Zhan et al., 2013). We therefore tested the assumption that plasticity-related mechanisms might occur at the timescale of meals in POMC neurons and contribute to short-term control of food intake.

RESULTS

The Postprandial State Increases the Activity of POMC Neurons via Synaptic Plasticity

We examined electrophysiological properties of POMC neurons according to prandial state in transgenic mice expressing the fluorescent protein tdTomato in POMC neurons ($POMC^{Cre:tdTomato}$ mice). $POMC^{Cre:tdTomato}$ mice were randomly assigned to three groups: one preprandial group with 2-h food restriction prior to the dark period and two postprandial groups that were further submitted to short-term, 1-h access to food at the beginning of the dark period (Figures S1A–S1C). Provided food corresponded to either a standard or a hypercaloric high-fat diet (diet compositions are given in Table S1). Body weight and blood levels of insulin, leptin, and acylated ghrelin did not differ statistically between mice (Figures S1D–S1G). This paradigm contrasts with the typical 24-h fasting model used to induce synaptic plasticity in AgRP and POMC neurons (Kong et al., 2016; Liu et al., 2012; Vong et al., 2011), for which body weight and circulating hormones are deeply altered (Figures S1B–S1G; Ahima et al., 1996).

We measured the electrical activity of POMC neurons using patch-clamp recordings in fresh brain slice preparations from $POMC^{Cre:tdTomato}$ mice in which POMC neurons were detected by fluorescence. $POMC^{Cre:tdTomato}$ neurons were recorded in cell-attached configuration, and spontaneous cell firing activity was recorded. We found that the firing rate of $POMC^{Cre:tdTomato}$ neurons was 3-fold higher in the postprandial group fed a standard diet for 1 h compared with the preprandial group (Figure 1A). POMC activity also increased when mice were fed a high-sucrose, low-fat diet for 1 h (Figure S1H). However, this increase was not found when mice were killed at the same time as those of the postprandial group but with no access to food (Figure S1I), indicating that the postprandial increase in POMC activity did not

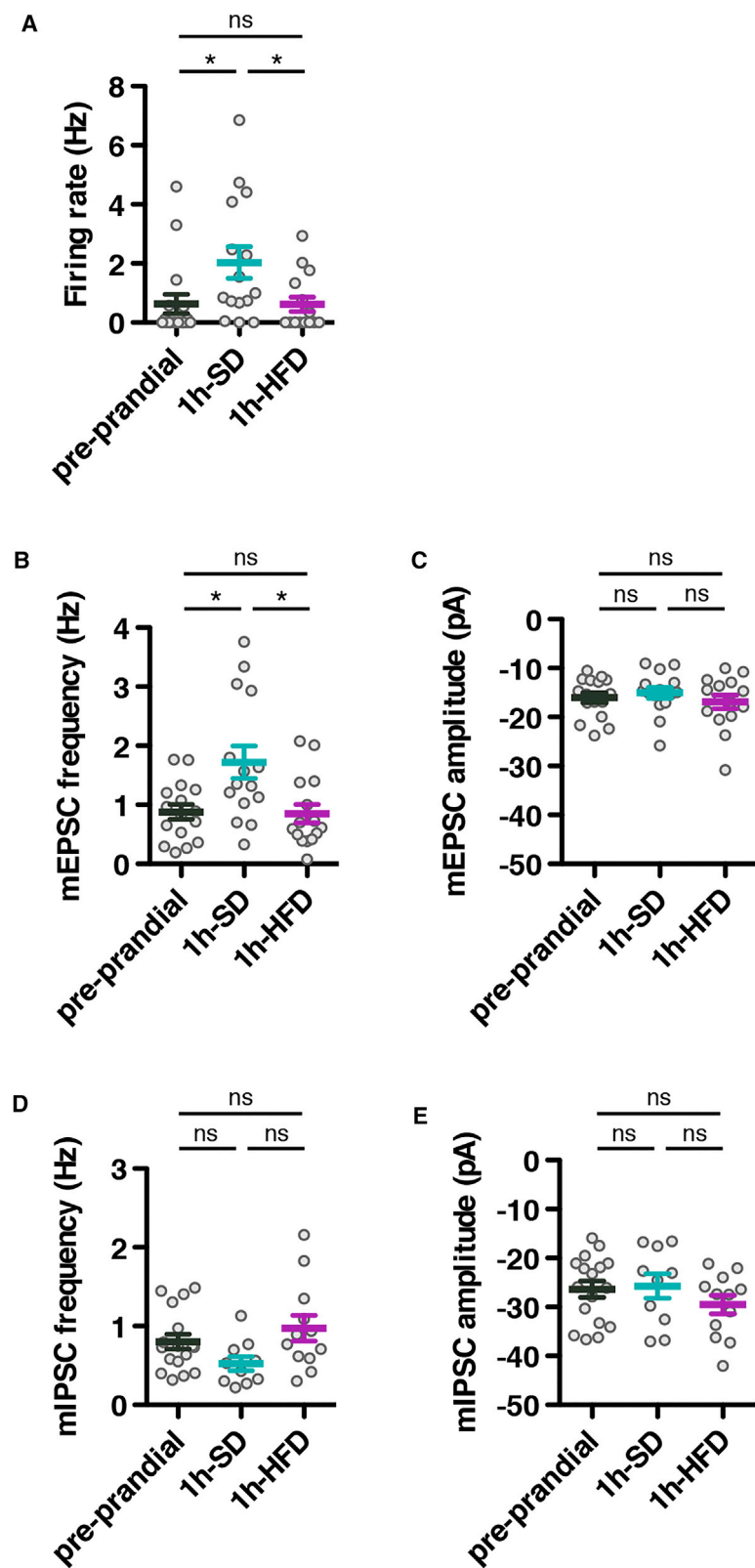depend on endogenous cycles or anticipatory processes but on food intake.

We next deciphered whether the postprandial hyperactivity of POMC neurons relies on presynaptic and/or postsynaptic changes by recording miniature excitatory and inhibitory postsynaptic currents (mEPSCs and mIPSCs, respectively) generated in POMC neurons. The frequency of miniature currents depends on the probability of release of neurotransmitters from presynaptic terminals, whereas their amplitude depends on postsynaptic receptor signaling. These currents were obtained by blocking overall spontaneous spiking activity in slices using tetrodotoxin and were recorded in whole-cell patch-clamp configuration. mEPSCs and mIPSCs were further isolated by blocking GABAergic and glutamatergic signaling, respectively. We found that the frequency of mEPSCs in $POMC^{Cre:tdTomato}$ neurons was doubled during the postprandial state (Figure 1B), but their amplitude was not significantly modified (Figure 1C). In contrast, the frequency and the amplitude of mIPSCs remained similar during the postprandial state (Figures 1D and 1E).

Thus, these results indicate that the activity of POMC neurons was regulated according to the prandial state. This regulation involves synaptic plasticity based on presynaptic changes that affects the excitatory tone applied on these neurons. This regulation was observed in response to a standard diet but not a high-fat hypercaloric diet, indicating that it depended on food composition (Figures 1A–1D).

The Postprandial State Induces Glial Retraction on POMC Neurons but Not Anatomical Remodeling of Synapses

Changes in energy availability promote physical synaptic rearrangement around AgRP and POMC neurons (Pinto et al., 2004). For instance, food deprivation stimulates excitatory synaptogenesis in AgRP neurons that contributes to increase the activity of these neurons during fasting (Kong et al., 2016; Liu et al., 2012). To investigate whether analogous structural plasticity occurred over the course of a meal, we performed post-mortem histological examination of brains from $POMC^{Cre:tdTomato}$ mice collected in the pre- or postprandial state. We first quantified synapses around arcuate POMC somata in fixed brain sections using electron microscopy. $POMC^{Cre:tdTomato}$ neurons were immunolabeled with electron-dense precipitates of diaminobenzidine, and synaptic contacts were counted (Figure 2A). We found that the synaptic density of $POMC^{Cre:tdTomato}$ neurons remained unchanged regardless of the prandial state of mice or the ingested diet (Figure 2B).

We next tested whether the ratio of excitatory to inhibitory synaptic inputs on POMC neurons varied according to the prandial state. We analyzed the type of presynaptic puncta around individual POMC somata by immunohistochemistry and confocal microscopy. Excitatory and inhibitory presynaptic terminals onto $POMC^{Cre:tdTomato}$ neurons were labeled using the VGluT1 (vesicular glutamate transporter 1) and VGAT (vesicular GABA transporter) markers, respectively (Figure 2C). No difference in the VGluT1:VGAT ratio on $POMC^{Cre:tdTomato}$ neurons was found between preprandial and postprandial groups on a standard diet (Figure 2D). Surprisingly, this ratio was dramatically increased with high-fat diet (HFD) exposure (Figure 2D), whereas the

A

The activity of POMC^Cre:tdTomato neurons was recorded in brain slices from mice in the preprandial or postprandial state. The firing rate was recorded in cell-attached configuration. Miniature excitatory postsynaptic current (mEPSC) and miniature inhibitory postsynaptic current (mIPSC) were recorded in whole-cell voltage-clamp configuration.

(A) Spontaneous firing rate in POMC^Cre:tdTomato neurons according to the prandial state. Preprandial mice (Pre), n = 17 cells from 4 mice; 1 h SD, n = 15 cells from 3 mice; 1 h HFD, n = 15 cells from 3 mice.

(B and C) Frequency (B) and amplitude (C) of mEPSCs in POMC^Cre:tdTomato neurons according to the prandial state. Pre, n = 16 cells from 9 mice; 1 h SD, n = 15 cells from 8 mice; 1 h HFD, n = 15 cells from 6 mice.

(D and E) Frequency (D) and amplitude (E) of mIPSCs in POMC^Cre:tdTomato neurons according to the prandial state. Pre, n = 17 cells from 4 mice; 1 h SD, n = 10 cells from 3 mice; 1 h HFD, n = 12 cells from 3 mice.

Data are means ± SEM. Statistical analyses were performed on recorded cells. Asterisks indicate statistical differences between groups: *$p < 0.05$. ns, no significant difference between groups. In (A), (B), and (D), data were analyzed using Kruskal-Wallis test followed by Dunn's test. In (C) and (E), data were analyzed using ANOVA followed by Newman-Keuls test.

B

C

D

E
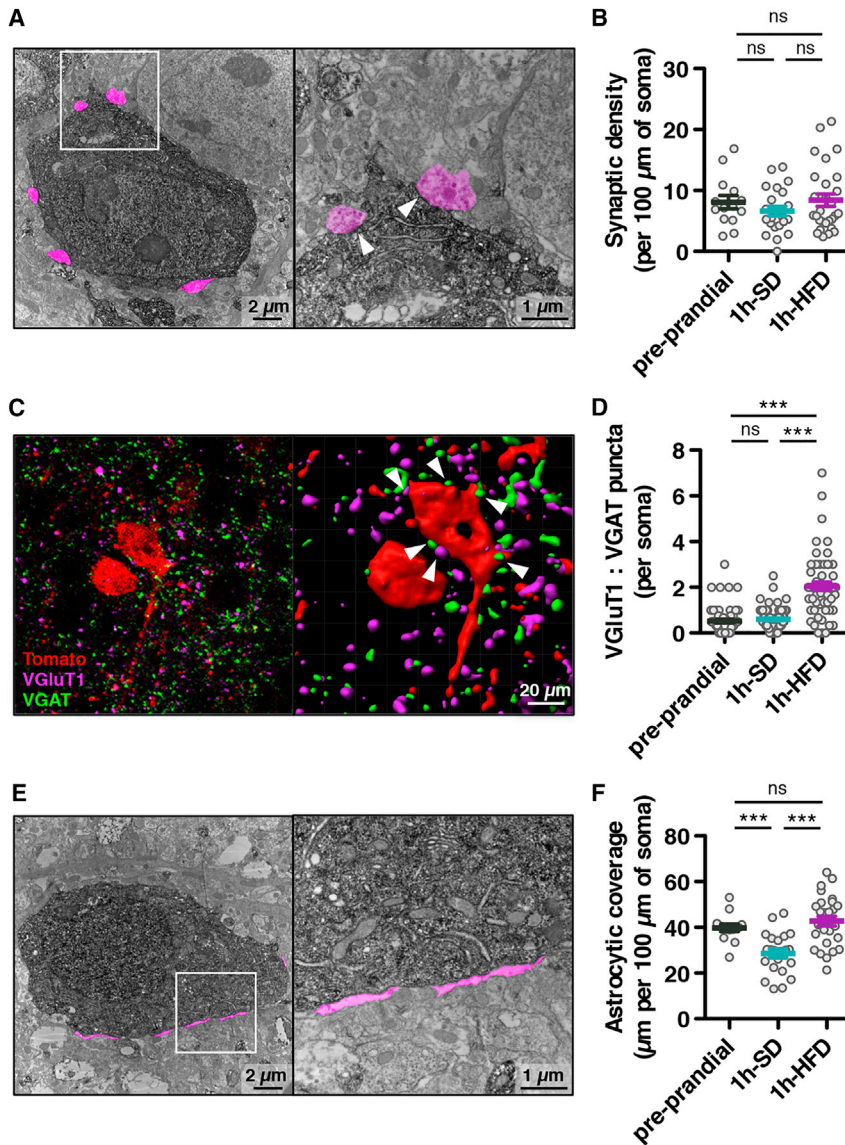
Figure 2. Neuroglial Interaction of $POMC^{Cre:tdTomato}$ Neurons Depends on the Prandial State

Cell interactions around $POMC^{Cre:tdTomato}$ neurons were determined by electron and confocal microscopy in fixed brain slices from mice in the pre-prandial or postprandial state.

(A) Image of arcuate $POMC^{Cre:tdTomato}$ neurons stained with diaminobenzidine by immunohistochemistry (in the dark) and acquired by electron microscopy at ×6,000 and ×30,000 magnification. Synapses around $POMC^{Cre:Tomato}$ neuron somata are pseudocolored in magenta (arrowheads point postsynaptic plaques).

(B) Synaptic density of $POMC^{Cre:tdTomato}$ neurons according to the prandial state. Synaptic density was measured on images acquired by electron microscopy at the original magnification of ×30,000. Pre, n = 14 cells from 3 mice; 1 h SD, n = 22 cells from 4 mice; 1 h HFD, n = 28 cells from 4 mice.

(C) Image of arcuate $POMC^{Cre:tdTomato}$ neurons (in red) surrounded by VGAT-immunoreactive (green) and VGluT1-immunoreactive (magenta) puncta, acquired by confocal microscopy. Puncta immediately adjacent to $POMC^{Cre:tdTomato}$ neurons (arrows) were counted after 3D rendering using Imaris software.

(D) Ratio of VGlut1:VGAT immunoreactive puncta adjacent to $POMC^{Cre:tdTomato}$ neuron somata. Pre, n = 62 cells from 3 mice; 1 h SD, n = 71 cells from 3 mice, 1 h HFD, n = 56 cells from 3 mice.

(E) Image of arcuate $POMC^{Cre:tdTomato}$ neurons (in the dark) acquired by electron microscopy at ×6,000 and ×30,000 magnification. Glial elements surrounding $POMC^{Cre:tdTomato}$ neuron somata are pseudocolored in magenta.

(F) Quantification of the astrocytic coverage on $POMC^{Cre:tdTomato}$ neurons according to the prandial state. Glial ensheathment on $POMC^{Cre:tdTomato}$ neurons was measured with ImageJ software on digitalized electron microscopy images acquired at the original magnification of ×30,000. Pre, n = 14 cells from 3 mice; 1 h SD, n = 22 cells from 4 mice; 1 h HFD, n = 28 cells from 4 mice. See also Table S2.

Data are means ± SEM. Statistical analyses were performed on labeled cells. Asterisks indicate statistical differences between groups: ***p < 0.001. In (B) and (D), data were analyzed using Kruskal-Wallis test followed by Dunn's test. In (F), data were analyzed using ANOVA followed by Newman-Keuls test.

POMC firing rate was not affected by the HFD at this time point (Figure 1A). The same results were obtained when ratios were computed from peri-somatic areas (Figure S2).

Astrocytes are integral components of synapses that also determine neurotransmission (Allen and Eroglu, 2017). Interestingly, astrocyte-POMC neurons interactions are sensitive to the metabolic state, and glial ensheathment seems to control POMC activity (Fuente-Martín et al., 2012; García-Cáceres et al., 2016; Kim et al., 2014). Thus we investigated whether changes in glial coverage occurred in response to food consumption. We used electron microscopy to assess the length of apposition of glial elements on arcuate diaminobenzidine-positive $POMC^{Cre:tdTomato}$ somata (Figure 2E). We found a significant reduction in astrocyte-POMC neuron interaction after exposure to 1-h standard diet feeding (Figure 2F; Table S2). Astrocyte coverage on POMC neurons was not affected by the HFD after 1 h (Figure 2F).

These results show that the number of synapses and the type of presynaptic puncta on POMC neurons were not changed by balanced food at the timescale of meals. Moreover, these data suggest that the postprandial hyperactivity of POMC following a standard meal might be linked to glial retraction from POMC neurons.

Postprandial Glial Retraction on POMC Neurons Requires Postprandial Hyperglycemia

Integration of meal-related signals in astrocytes can modify interaction with POMC neurons (García-Cáceres et al., 2016;
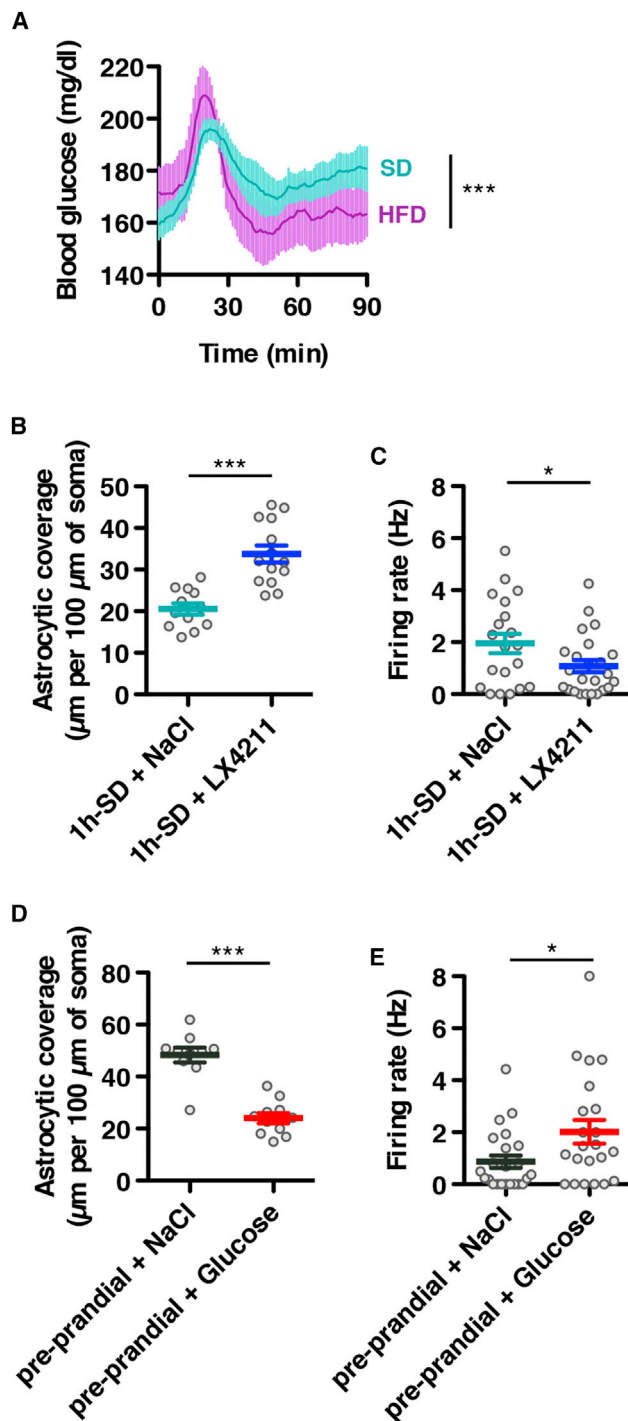
Figure 3. Neuroglial Interaction of *POMC*^{Cre:tdTomato} Neurons Depends on Blood Glucose Level

(A) Blood glucose excursion during standard and HFD consumption. Blood glucose was measured in real time using telemetric implants (n = 5 mice). See also Figure S2.

(B) Quantification of astrocytic coverage on *POMC*^{Cre:tdTomato} neurons during the postprandial state in mice fed an SD and treated with NaCl or 10 mg/kg LX4211, a dual SGLT1/SGLT2 inhibitor (intraperitoneal [i.p.] injection). 1 h SD + NaCl, n = 10 cells from 3 mice; 1 h SD + LX4211, n = 14 cells from 3 mice.

Kim et al., 2014). Here we tested whether postprandial elevation of blood glucose mediated the neuroglial remodeling we observed on a standard diet. We first continuously monitored glycemia of mice following food consumption by telemetry using glucometer implants. Despite some differences in postprandial blood glucose excursions that reflect the specific glycemic index of the diets, glycemia increased with either a standard diet or HFD, peaking similarly 20–22 min after food introduction, confirming a regulated postprandial hyperglycemic response after food consumption (Figure 3A; Figure S3A). To appreciate the role of postprandial hyperglycemia on neuroglial plasticity, mice fed a standard diet were pretreated with LX4211, a dual inhibitor of SGLT1/SGLT2 transporters that inhibits intestinal absorption and renal reabsorption of glucose (Powell et al., 2014; Powell et al., 2013), or with saline (Figure S3B). Intraperitoneal injection of LX4211 (10 mg/kg) prior to standard diet exposure limited the hyperglycemic response in comparison with saline pretreatment (Figures S3C and S3D). Remarkably, LX4211 pretreatment inhibited both standard diet-induced astrocytic retraction on arcuate *POMC*^{Cre:tdTomato} neurons (Figure 3B) and the related increase in arcuate *POMC*^{Cre:tdTomato} neuron activity (Figure 3C). Thus, postprandial neuroglial plasticity of POMC neurons required a surge of blood glucose.

We next tested whether elevation of blood glucose was sufficient to trigger neuroglial remodeling. We treated mice with an intraperitoneal injection of glucose (0.5 g/kg) or saline instead of giving them a standard diet (Figure S3E). This glucose load mimicked the glycemic response induced by standard diet ingestion (Figures S3F and S3G). Notably, we found a drastic astrocytic retraction on arcuate *POMC*^{Cre:tdTomato} neurons in glucose-treated mice in comparison with control mice (Figure 3D). The glucose load also increased the firing rate of these neurons (Figure 3E). Thus, glucose administration recapitulated the effects found in response to standard diet ingestion.

Together, these results demonstrate that glucose signaling was both necessary and sufficient for postprandial neuroglial plasticity and activation of POMC neurons.

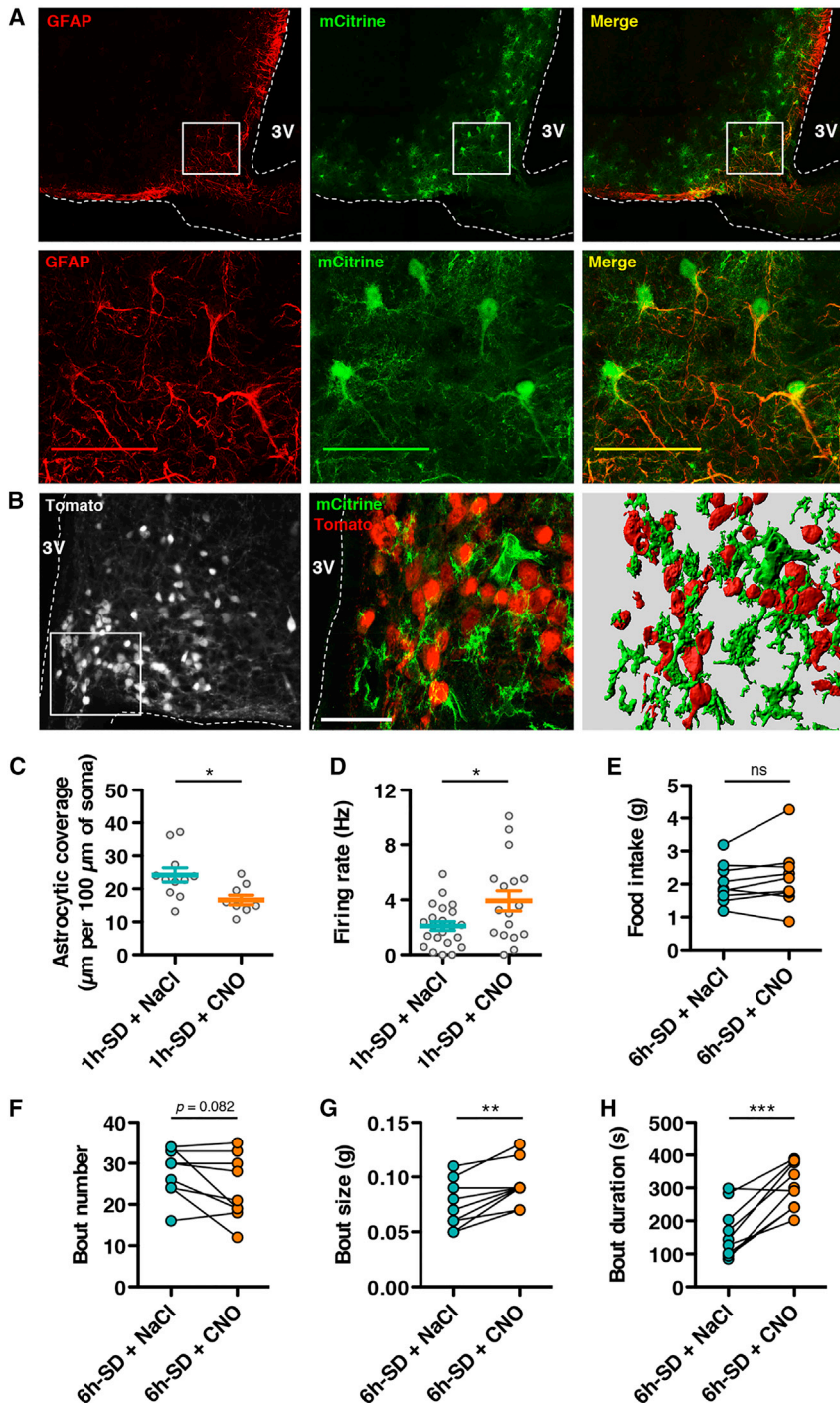## Glial Retraction on POMC Neurons Alters Feeding Behavior

To evaluate the behavioral outcome of the postprandial neuroglial plasticity of POMC neurons, we thought to interfere in the remodeling activity of astrocytes during feeding. Astrocytic

(C) Firing rate of *POMC*^{Cre:tdTomato} neurons during the postprandial state in mice fed an SD and treated with NaCl or LX4211. 1 h SD + NaCl, n = 20 cells from 3 mice; 1 h SD + LX4211, n = 24 cells from 4 mice.

(D) Quantification of astrocytic coverage on *POMC*^{Cre:tdTomato} neurons in food-restricted mice treated with NaCl or 0.5 g/kg glucose (i.p. injection). Pre + NaCl, n = 10 cells from 3 mice; Pre + glucose, n = 11 cells from 3 mice.

(E) Firing rate of *POMC*^{Cre:tdTomato} neurons in food-restricted mice treated with NaCl or glucose. Pre + NaCl, n = 23 cells from 5 mice; Pre + glucose, n = 22 cells from 5 mice.

Data are means ± SEM. Asterisks indicate statistical differences between groups: *p < 0.05 and ***p < 0.001. In (A), data were analyzed using two-way ANOVA. In (B)–(D), analyses were performed on labeled or recorded cells, and data were analyzed using two-tailed unpaired Student's test. In (D), analysis was performed on recorded cells, and data were analyzed using two-tailed Mann-Whitney test.

Figure 4. Chemogenetically Induced Glial Retraction on *POMC*^Cre:tdTomato Neurons Stimulates POMC Neurons Activity and Influences Feeding Behavior

Mice were infused bilaterally with rAAV8/GFAP-Ha-hM4D(Gi)-IRES-mCitrine particles into the arcuate nucleus of the hypothalamus. rAAV8/GFAP-Ha-hM4D(Gi)-IRES-mCitrine particles express the Gi-coupled hM4D receptor and mCitrine reporter under control of GFAP promoter.

(A) Representative images showing mCitrine immunoreactivity (green) overlapping with glial fibrillary acidic protein (GFAP) staining (red). Images were acquired with a confocal microscope using ×10 and ×63 oil immersion objectives. 3V, third ventricle. Scale bar, 30 μm.

(B) Representative images showing adeno-associated virus (AAV)-transduced mCitrine-positive cells (green) enwrapping arcuate Tomato-positive *POMC*^Cre:tdTomato somata (red). Images were acquired with a ×63 oil immersion objective on a confocal microscope, and volume rendering was done using Imaris software. Scale bar, 30 μm.

(C) Quantification of astrocytic coverage on *POMC*^Cre:tdTomato neurons during the postprandial state in hM4D(Gi)-transduced mice fed an SD diet and treated with NaCl or 1 mg/kg CNO (i.p. injection). 1 h SD + NaCl, n = 11 cells from 3 mice; 1 h SD + CNO, n = 9 cells from 3 mice.

(D) Firing rate of *POMC*^Cre:tdTomato neurons during the postprandial state in hM4D(Gi)-transduced mice fed an SD and treated with NaCl or CNO. 1 h SD + NaCl, n = 22 cells from 5 mice; 1 h SD + CNO, n = 17 cells from 5 mice.

(E) Cumulative food intake during a 6-h period in hM4D(Gi)-transduced mice fed a SD and treated with NaCl or 1 mg/kg CNO (i.p. injection) (n = 9 mice).

(F–H) Feeding parameters of hM4D(Gi)-transduced mice (n = 9) treated with NaCl or CNO, including number of feeding events (F), size of feeding bouts (G) and duration of feeding bouts (H).

In (C) and (D), data are means ± SEM. Asterisks indicate statistical differences between groups: *p < 0.05, **p < 0.01, and ***p < 0.001. In (C) and (D), analyses were performed on labeled or recorded cells, and data were analyzed using two-tailed unpaired Student's test. In (E) and (H), data were analyzed using two-tailed paired Student's test.

morphology is dynamically regulated by the cyclic AMP signaling pathway (Vardjan et al., 2014). We took advantage of designer receptors exclusively activated by designer drugs (DREADD)-based chemogenetics (Roth, 2016) to selectively manipulate intracellular cAMP of astrocytes in adult animals. We chose to express the Gi-coupled designer receptor hM4D under control of the astrocytic glial fibrillary acidic protein (GFAP) promoter using viral particles containing the Gi-coupled DREADD construct fused to the mCitrine reporter (rAAV8/GFAP-Ha-hM4D(Gi)-IRES-mCitrine). This system efficiently inhibited cAMP signaling in primary cultures of murine astrocytes when activated by the clozapine N-oxide (CNO) ligand (Figure S4). Viral particles containing the DREADD construct were stereotactically injected into the arcuate nucleus of the hypothalamus. Post-mortem inspection of some injected brains revealed efficient targeting of the arcuate nucleus and showed that GFAP-positive mCitrine-transduced cells exhibited a stellate morphology consistent with that of astrocytes (Figure 4A). Moreover, several

mCitrine-transduced cells enwrapped Tomato-positive cells (Figure 4B), suggesting close interaction between transduced astrocytes and arcuate POMC neurons. Of note, immunodetection of Tomato-positive cells revealed no overlap with mCitrine staining, confirming the specificity of transduction (Figure 4B).

We then studied astrocyte-POMC interaction in the postprandial state upon CNO treatment. DREADDed POMC^Cre:tdTomato mice received a single intraperitoneal injection of CNO (1 mg/kg) prior to standard diet exposure (Figure S4C). Control mice received a saline injection. We found that postprandial astrocytic coverage on POMC^Cre:tdTomato neurons from DREADDed mice injected with saline was low (Figure 4C), at a level similar to that obtained previously in POMC^Cre:tdTomato mice without DREADD (Figure 2F). This result shows that DREADD transduction did not alter the ability of arcuate astrocytes to retract in response to standard diet ingestion. Interestingly, CNO did not inhibit this postprandial response but further increased glial retraction on POMC neurons (Figure 4C). These results suggest that CNO-mediated activation of arcuate astrocyte Gi signaling inhibited astrocyte-POMC neuron contacts.

We next assessed the effect of CNO injection on state-dependent activity of POMC neurons. As before, DREADDed POMC^Cre:tdTomato mice received a single intraperitoneal injection of CNO (1 mg/kg) or saline before exposure to a standard diet for 1 h, and the brains were processed for electrophysiology. We found that the postprandial firing rate of POMC^Cre:tdTomato neurons was elevated in DREADDed mice injected with saline (Figure 4D) and was similar to that in POMC^Cre:tdTomato mice without DREADD (Figure 1A), showing that DREADD transduction did not alter POMC neuron functioning. In contrast, CNO pretreatment in DREADDed mice further increased the postprandial firing rate in POMC^Cre:tdTomato neurons (Figure 4D). These results further suggest that CNO-mediated activation of arcuate astrocyte Gi signaling could also stimulate the activity of POMC neurons.

We finally investigated feeding behavior in DREADDed POMC^Cre:tdTomato mice. Mice received a single injection of CNO or saline before food introduction, and feeding behavior was monitored over a 24-h period. At the 6-h time point, the behavioral effects of CNO were maximal. CNO pretreatment did not influence the cumulative food intake (Figure 4E), but it significantly changed the temporal organization of the feeding behavior. Although number of feeding bouts tended to decrease upon CNO administration (Figure 4F), the size of the bouts was strongly increased by the treatment. Notably, CNO increased the amount of ingested food per feeding bout (Figure 4G) and the duration of the feeding bout (Figure 4H). These effects were not detectable during the first 1-h period of feeding (Figures S4D–S4G), became significant after 3 h (Figures S4H–S4K), and decreased but were still significant after 24 h (Figures S4L–S4O).

We checked the behavioral effects of CNO per se in POMC^Cre:tdTomato DREADD-free mice. One single intraperitoneal injection of 1 mg/kg CNO in unDREADDed POMC^Cre:tdTomato mice did not produced any changes in the feeding behavior (Figures S5A–S5D), confirming that CNO alone is pharmacologically and behaviorally inert in mice (Alexander et al., 2009; Armbruster et al., 2007; Farrell et al., 2013; Guettier et al., 2009; Krashes et al., 2011) and that CNO-to-clozapine back-metabolism is low in mice, with blood clozapine being negligible when CNO is dosed at 1 mg/kg (Farrell et al., 2013; Manvich et al., 2018). CNO treatment in POMC^Cre:tdTomato DREADD-free mice did not modify the firing rate of POMC neurons after 1-h standard diet (SD) feeding (Figure S5E).

We also tested whether CNO treatment influenced general ambulatory ability and emotionality in DREADDed POMC^Cre:tdTomato mice, two parameters that can affect feeding behavior. Locomotor activity and anxiety-like behavior upon CNO treatment were assessed in a wall-enclosed open field arena (Walsh and Cummins, 1976). Following CNO or saline injection, mice were fed for 3 h and then placed in the arena during a 30-min trial (Figure S5F). CNO did not alter the total ambulatory distance of mice (Figure S5G) and did not change the number of entries in the inner zone (Figure S5H) or the time spent in this zone versus the periphery (Figure S5I). These data indicate that a single injection of 1 mg/kg CNO in mice did not produce sedative and anxiolytic effects at a time when feeding behavior was modified.

Altogether, these results indicate that CNO treatment was effective in altering the temporal pattern of meals in DREADDed mice without changing locomotor activity or emotionality and that this effect required Gi signaling in hypothalamic astrocytes.

DISCUSSION

In this study, we show that the electrical activity of arcuate POMC neurons is regulated according to the prandial state. Using electrophysiological recordings from acute brain slices, we evidenced the postprandial hyperactivity of these neurons. These data are consistent with those obtained in awake mice using direct in vivo recording, showing rapid and sustained changes in POMC activity during feeding (Chen et al., 2015; Mandelblat-Cerf et al., 2015). In addition, we found that postprandial hyperactivity of POMC neurons engages presynaptic modifications affecting the excitatory tone applied on these neurons. Such state-dependent plasticity in the melanocortin system has already been established in response to changes in nutritional state (Dietrich and Horvath, 2013; Zeltser et al., 2012). However, until then, this phenomenon has been found only after high metabolic challenges, including starvation (Liu et al., 2012; Vong et al., 2011; Yang et al., 2011) and overfeeding (Benani et al., 2012). Here we report that synaptic plasticity on POMC neurons can be recapitulated at the timescale of meals in freely behaving mice in a physiological context, meaning that this process is not only an adaptive mechanism elicited during extreme and perhaps rare metabolic situations but also develops during day-to-day life in response to subtle metabolic changes.

To evidence synaptic plasticity in POMC neurons at the timescale of meals, we used ex vivo electrophysiology in living brain slices. This approach has been widely used to reveal and study the plasticity of the melanocortin system in response to many metabolic changes, including those related to aging, obesity, hormone treatment, fasting, overfeeding, or physical activity (Baquero et al., 2015; Benani et al., 2012; Dodd et al., 2018; He et al., 2018; Liu et al., 2012; Newton et al., 2013; Pinto et al., 2004; Suyama et al., 2017; Vong et al., 2011; Yang et al., 2011,

2012). *Ex vivo* electrophysiological approaches are also efficient for investigating changes in neurotransmission induced by brief nutritional challenges, and it has been shown that 1-h HFD was sufficient to occlude insulin-induced plasticity in dopamine neurons of the ventral tegmental area (Labouèbe et al., 2013). In the present study, postprandial electrophysiological changes that occur in POMC neurons *in vivo* were not lost during *ex vivo* preparation, which includes short transfer in high-glucose ice-cold preservation medium. Thus, this result supports the idea that postprandial presynaptic changes are triggered by hard, long-lasting remodeling processes.

Neuroanatomical analyses revealed that postprandial hyperactivity of POMC neurons when consuming an SD is not associated with structural synaptic remodeling. The absence of postprandial synaptic re-organization onto POMC somata has been confirmed by two independent scores from electron or confocal microscopic images. Both approaches gave similar results, indicating no change in the number and type of synapses after feeding standard food. However, starvation requires spinogenesis to increase the excitatory tone on orexigenic AgRP neurons (Kong et al., 2016; Liu et al., 2012). Limitations of our study include the fact that synaptic counting was performed on POMC somata or peri-somatic areas only. Thus, we cannot exclude synaptic remodeling far from somata, in the dendritic arborization. Moreover, to examine the type of synapses impinging on POMC neurons, we stained presynaptic puncta only. Although the method is appropriate to appreciate a shift between excitatory and inhibitory terminals onto neurons, quantification of presynaptic puncta does not denote *bona fide* bi-partite synapses because presynaptic puncta may be present without being co-localized with a postsynaptic marker. This methodological issue limits the accuracy of the measure. Nevertheless, this method is sensitive enough to highlight morphological remodeling in a neuronal system, either in the melanocortin system or elsewhere (Baquero et al., 2015; Cristino et al., 2013; Melnick et al., 2007; Newton et al., 2013). Keeping these issues in mind, our histological data are in favor of an absence of morphological remodeling of presynaptic terminals onto POMC neurons after a standard meal. Indeed, constant effervescence for molding new synapses and eliminating others to generate new configurations at the timescale of meals would represent a high cost for the organism.

In many neuroendocrine systems, modification of astrocyte coverage on synapses is a way to efficiently and rapidly modulate the synaptic strength onto neurons with no need of building new synapses (Clasadonte and Prevot, 2018; Oliet et al., 2001, 2002; Theodosis et al., 2008). Time-lapse imaging shows that peri-synaptic astrocytic processes that embrace synapses are highly reactive and motile structures, to an even higher degree than dendritic spines (Bernardinelli et al., 2014). Furthermore, astrocytes surrounding POMC and AgRP somata are known to change their morphology according to metabolic cues (Fuente-Martín et al., 2012; García-Cáceres et al., 2016, 2019; Horvath et al., 2010; Kim et al., 2014). Here we found that consumption of standard food induced robust glial retraction around POMC somata, showing that structural astroglial plasticity happens over the course of meals. Moreover, glial retraction was invariably associated with an increase in POMC firing rate, as was the case after feeding an SD but also after glucose injection or

chemogenetic manipulation. Inversely, large glial coverage was detected during the preprandial state or after feeding an HFD, two situations where POMC activity was low. These results suggest the existence of a structure-function relationship in the astrocyte/POMC dyad. This is consistent with previous reports showing massive glial ensheathment of POMC neurons associated with reduced functioning of POMC neurons during diet-induced obesity (Enriori et al., 2007; Horvath et al., 2010; Paeger et al., 2017). Furthermore, we found that more than 80% of POMC neurons undergo postprandial astrocytic retraction after a standard meal. The low variability in this response contrasts with the well-known heterogeneity of POMC neurons (Dodd et al., 2018; Lam et al., 2017; Sohn and Williams, 2012; Williams et al., 2010). Thus, our data suggest that taking into account the prandial state of animals could minimize the apparent functional heterogeneity of POMC neurons.

In this study, we used chemogenetic tools to interrogate the function of hypothalamic astrocytes. As already reported by others (Jones et al., 2018), we found that artificial chemogenetic manipulation with the inhibitory hM4D(Gi) receptor rapidly reduces intracellular cyclic AMP in GFAP-expressing cells such as astrocytes. We also found that CNO injection in mice transduced with the inhibitory DREADD induced robust glial retraction around POMC somata. This is consistent with previous pharmacological studies showing that astrocyte stellation is regulated within minutes by intracellular cyclic AMP level (Vardjan et al., 2014). Accordingly, postprandial neuroglial plasticity might implicate a cyclic AMP-dependent signaling pathway in astrocytes. In addition, a change in blood glucose appears to be crucial to initiate postprandial glial retraction. Although we did not determine whether this process requires direct astrocytic glucose sensing, this result is consistent with others showing that glial cells can be shaped by glycemic fluctuations (Daumas-Meyer et al., 2018; Langlet et al., 2013). Specifically, these data complete the current model in which hypothalamic astrocytes respond to metabolic cues, including leptin and insulin, to adjust the activity of the melanocortin system via changes in astrocyte-neuron interaction and, ultimately, to maintain energy homeostasis (García-Cáceres et al., 2016; Kim et al., 2014). In addition, we show that this glucose-dependent neuroglial plasticity can be initiated during normal physiology at the timescale of meals. Moreover, we found that *in vivo* activation of the CNO/hM4D(Gi) system expressed in arcuate GFAP-expressing cells stimulated activity of POMC neurons. Using similar GFAP-driven chemogenetic tools, other groups have reported previously that application of CNO acutely on brain slices modifies the firing rate of AgRP and POMC neurons, confirming that astrocytes control the activity of the melanocortin system (Chen et al., 2016; Yang et al., 2015). In our work, DREADD-mediated activation of Gq signaling has not been examined. GFAP-driven hM3D(Gq) viral particles have been used successfully to study gliotransmission in a neuronal system (Adamsky et al., 2018; Agulhon et al., 2013; Scofield et al., 2015) and arcuate astrocyte-AgRP/POMC neuron interaction more specially (Chen et al., 2016; Yang et al., 2015). At the molecular level, the effects of hM3D(Gq) activation are likely to be mediated by intracellular Ca^{2+} elevation in astrocytes (Adamsky et al., 2018; Agulhon et al., 2013; Bonder and McCarthy, 2014; Chen et al., 2016).

On the other hand, activation of hM4D(Gi) is known to decrease cAMP level in cells (Armbruster et al., 2007; Jones et al., 2018), which was confirmed in the present study. Interestingly, activation of Gq- and Gi-coupled DREADD receptors produces opposite effects in neurons, such as neuronal firing or silencing (Armbruster et al., 2007). In astrocytes, these tools elevate calcium and stimulate gliotransmission similarly (Durkee et al., 2019). Thus, the physiological effects of Gq- and Gi-coupled DREADD receptors in astrocytes are not as straightforward as in neurons, and additional studies are needed to characterize the molecular signaling pathways in astrocytes that regulate hunger state.

At the behavioral level, activation of the CNO/hM4D(Gi) system in arcuate astrocytes did not affect total food intake. This corroborates previous studies showing that chemogenetic manipulation of hypothalamic astrocytes via Gi signaling does not alter basal food intake (Chen et al., 2016; Yang et al., 2015). However, further examination of feeding behavior revealed that activation of the CNO/hM4D(Gi) system in glia induced larger but less frequent feeding bouts over the next few hours, suggesting that arcuate astrocytes contribute to satiety. This behavioral effect might rely on the associated hyperactivity of POMC neurons induced by the treatment. A role of POMC neurons in control of satiety has already been evidenced elsewhere (Fenselau et al., 2017; Richard et al., 2011). This does not rule out a concomitant effect on adjacent AgRP neurons and on arcuate glutamatergic neurons, which are also involved in the control of satiety (Chen et al., 2016; Fenselau et al., 2017; Yang et al., 2015). Interestingly, CNO-induced behavioral effects appeared after a delay of few hours and were maximal 6 h post-CNO injection, suggesting that postprandial neuroglial plasticity is not involved in termination of the first feeding bouts but affects hunger slowly. This also argues for involvement of arcuate POMC neurons in CNO-induced behavioral effects because these neurons are known to alter feeding behavior long term (Aponte et al., 2011; Zhan et al., 2013). Together, our data strongly suggest that glial retraction onto POMC neurons is part of the slow and sustained neurobiological mechanisms that contribute to control of satiety.

We also found that postprandial changes in mEPSC frequency in POMC neurons were not in line with those of the VGluT:VGaT ratio on POMC somas. Actually, the VGluT:VGaT ratio remained unchanged after a standard meal, whereas mEPSC frequency increased. Because a reduction in astrocytic coverage was found simultaneously, this result suggests a prominent role of the dynamic glial response in regulation of POMC activity after a meal instead of a synaptic rearrangement on POMC neurons. In support of this, recent studies have shown that astrocytes can directly activate POMC neurons (Bouyakdan et al., 2019; Sweeney et al., 2016). Furthermore, an elegant study performed in hippocampal neurons has shown that astrocyte activity is not only necessary for synaptic plasticity but can be sufficient to generate *de novo* synaptic plasticity (Adamsky et al., 2018). Inversely, we found that 1-h HFD feeding induced a robust synaptic switch around POMC neurons, increasing excitatory and decreasing inhibitory synaptic puncta on POMC somata, whereas the net firing rate of POMC neurons as well as the frequency of miniature currents

remained unchanged. The discrepancy between the functional and histological analyses probably reflects a delay for novel synapses to be operative. Again, in this study, we quantified presynaptic puncta, and it does not denote *bona fide* synapses. Thus, more accurate identification of mature synapses, by labeling post-synaptic elements, for instance, would help to clarify. Nevertheless, the structural synaptic remodeling found here after 1-h HFD feeding, increasing excitatory inputs on POMC neurons, likely represents an adaptive response against energy balance deviation and excessive calorie intake. In fact, forced consumption of an HFD for a few days firmly increases POMC neuron activity according to synaptic plasticity-related processes (Benani et al., 2012; Suyama et al., 2017), which is in line with the early synaptic remodeling found here.

Strikingly, consumption of an HFD for 1 h did not modify the activity of POMC neurons. Furthermore, HFD did not change excitatory and inhibitory tones applied on POMC neurons or cause glial retraction. Thus, postprandial functional and structural changes on POMC neurons were essentially lost when consuming high-fat, energy-dense foods. This lack of effect appears not to be linked to food neophobia because mice were trained with an HFD before the trial, ate normal amounts of food during the trial, and displayed postprandial hyperglycemia. Moreover, HFD-related signals were sensed in the brain, as evidenced by the HFD-induced synaptic switch around POMC somata. Rather, these results suggest that postprandial neuroglial plasticity integrates food composition. This result is also in line with a recent study showing that macronutrients produce specific effects on the melanocortin system (Su et al., 2017), with gastro-intestinal infusion of glucose resulting in higher and more prolonged reduction of AgRP neuron activity than lipids. According to the present study, in mice kept on an SD, blood glucose was required to trigger glial retraction. Because the HFD also raised glycemia, why did it not initiate such postprandial neuroglial plasticity? In contrast to that on the SD, HFD-induced hyperglycemia was very brief and returned to basal values as soon as 30–40 min, whereas glycemia was still elevated after 1 h on the SD (Figure 3A). Thus, one can propose that long-lasting elevation of glycemia is critical to provoke morphological changes in hypothalamic astrocytes and to activate POMC neurons. However, we observed that 1-h exposure to a high-sucrose, low-fat diet, which contains fast-release carbohydrates like those in the HFD, or a single intraperitoneal injection of glucose increased the POMC firing rate as well. Accordingly, blood glucose kinetics would not be key factors for neuroglial plasticity, and a low glycemic index does not appear to be an indispensable prerequisite to activate POMC neurons. Another possibility is that interfering factors derived from the HFD but not from the SD, such as lipids or inflammatory mediators, might have inhibited the response. Further studies are needed to understand this specificity. In all cases, postprandial neuroglial plasticity appears to be a slow, macronutrient-dependent mechanism that produces delayed effects on food intake and follows fast, macronutrient-independent integration of post-ingestive signals (Beutler et al., 2017; Su et al., 2017). In this scheme, satietogenic properties of macronutrients would be also based on their ability to induce neuroglial remodeling.

In conclusion, these findings reveal that neuroglial plasticity within circuits controlling appetite happens at the timescale of meals. Moreover, our results strongly suggest that dynamic interactions between neurons and glial cells influence feeding behavior. Finally, this macronutrient-dependent plasticity provides a neurobiological basis for satiety, and alteration of this mechanism might be a factor in maladaptive eating disorders and obesity.

STAR★METHODS

Detailed methods are provided in the online version of this paper and include the following:

- KEY RESOURCES TABLE
- LEAD CONTACT AND MATERIALS AVAILABILITY
- EXPERIMENTAL MODEL AND SUBJECT DETAILS
    - Mice
    - Experimental design
    - Primary astrocyte culture
- METHOD DETAILS
    - Stereotactic injections
    - Drug administration
    - Blood biochemistry
    - Continuous monitoring of feeding behavior
    - Continuous monitoring of glycemia
    - Open Field Test
    - Electrophysiology
    - Electron microscopy
    - Confocal microscopy
    - Image analysis
    - Cytotoxicity assay in primary astrocyte culture
    - cAMP assay in primary astrocyte culture
- QUANTIFICATION AND STATISTICAL ANALYSIS
- DATA AND CODE AVAILABILITY

SUPPLEMENTAL INFORMATION

Supplemental Information can be found online at https://doi.org/10.1016/j.celrep.2020.02.029.

DECLARATION OF INTERESTS

The authors declare no competing interests.

REFERENCES

Adamsky, A., Kol, A., Kreisel, T., Doron, A., Ozeri-Engelhard, N., Melcer, T., Refaeli, R., Horn, H., Regev, L., Groysman, M., et al. (2018). Astrocytic Activation Generates De Novo Neuronal Potentiation and Memory Enhancement. Cell *174*, 59–71.e14.

Agulhon, C., Boyt, K.M., Xie, A.X., Friocourt, F., Roth, B.L., and McCarthy, K.D. (2013). Modulation of the autonomic nervous system and behaviour by acute glial cell Gq protein-coupled receptor activation in vivo. J. Physiol. *591*, 5599–5609.

Ahima, R.S., Prabakaran, D., Mantzoros, C., Qu, D., Lowell, B., Maratos-Flier, E., and Flier, J.S. (1996). Role of leptin in the neuroendocrine response to fasting. Nature *382*, 250–252.

Alexander, G.M., Rogan, S.C., Abbas, A.I., Armbruster, B.N., Pei, Y., Allen, J.A., Nonneman, R.J., Hartmann, J., Moy, S.S., Nicolelis, M.A., et al. (2009). Remote control of neuronal activity in transgenic mice expressing evolved G protein-coupled receptors. Neuron *63*, 27–39.

Allen, N.J., and Eroglu, C. (2017). Cell Biology of Astrocyte-Synapse Interactions. Neuron *96*, 697–708.

Aponte, Y., Atasoy, D., and Sternson, S.M. (2011). AGRP neurons are sufficient to orchestrate feeding behavior rapidly and without training. Nat. Neurosci. *14*, 351–355.

Armbruster, B.N., Li, X., Pausch, M.H., Herlitze, S., and Roth, B.L. (2007). Evolving the lock to fit the key to create a family of G protein-coupled receptors potently activated by an inert ligand. Proc. Natl. Acad. Sci. USA *104*, 5163–5168.

Atasoy, D., Betley, J.N., Su, H.H., and Sternson, S.M. (2012). Deconstruction of a neural circuit for hunger. Nature *488*, 172–177.

Baquero, A.F., Kirigiti, M.A., Baquero, K.C., Lee, S.J., Smith, M.S., and Grove, K.L. (2015). Developmental changes in synaptic distribution in arcuate nucleus neurons. J. Neurosci. *35*, 8558–8569.

Benani, A., Hryhorczuk, C., Gouazé, A., Fioramonti, X., Brenachot, X., Guissard, C., Krezymon, A., Duparc, T., Colom, A., Nédélec, E., et al. (2012). Food intake adaptation to dietary fat involves PSA-dependent rewiring of the arcuate melanocortin system in mice. J. Neurosci. *32*, 11970–11979.

Bernardinelli, Y., Randall, J., Janett, E., Nikonenko, I., König, S., Jones, E.V., Flores, C.E., Murai, K.K., Bochet, C.G., Holtmaat, A., and Muller, D. (2014). Activity-dependent structural plasticity of perisynaptic astrocytic domains promotes excitatory synapse stability. Curr. Biol. *24*, 1679–1688.

Beutler, L.R., Chen, Y., Ahn, J.S., Lin, Y.C., Essner, R.A., and Knight, Z.A. (2017). Dynamics of Gut-Brain Communication Underlying Hunger. Neuron *96*, 461–475.e5.

Bonder, D.E., and McCarthy, K.D. (2014). Astrocytic Gq-GPCR-linked IP3R-dependent Ca2+ signaling does not mediate neurovascular coupling in mouse visual cortex in vivo. J. Neurosci. 34, 13139–13150.

Bouyakdan, K., Martin, H., Liénard, F., Budry, L., Taib, B., Rodaros, D., Chrétien, C., Biron, É., Husson, Z., Cota, D., et al. (2019). The gliotransmitter ACBP controls feeding and energy homeostasis via the melanocortin system. J. Clin. Invest. 129, 2417–2430.

Brenachot, X., Rigault, C., Nédélec, E., Laderrière, A., Khanam, T., Gouazé, A., Chaudy, S., Lemoine, A., Datiche, F., Gascuel, J., et al. (2014). The histone acetyltransferase MOF activates hypothalamic polysialylation to prevent diet-induced obesity in mice. Mol. Metab. 3, 619–629.

Brenachot, X., Gautier, T., Nédélec, E., Deckert, V., Laderrière, A., Nuzzaci, D., Rigault, C., Lemoine, A., Pénicaud, L., Lagrost, L., and Benani, A. (2017). Brain Control of Plasma Cholesterol Involves Polysialic Acid Molecules in the Hypothalamus. Front. Neurosci. 11, 245.

Chen, Y., Lin, Y.C., Kuo, T.W., and Knight, Z.A. (2015). Sensory detection of food rapidly modulates arcuate feeding circuits. Cell 160, 829–841.

Chen, N., Sugihara, H., Kim, J., Fu, Z., Barak, B., Sur, M., Feng, G., and Han, W. (2016). Direct modulation of GFAP-expressing glia in the arcuate nucleus bi-directionally regulates feeding. eLife 5.

Clasadonte, J., and Prevot, V. (2018). The special relationship: glia-neuron interactions in the neuroendocrine hypothalamus. Nat. Rev. Endocrinol. 14, 25–44.

Cristino, L., Busetto, G., Imperatore, R., Ferrandino, I., Palomba, L., Silvestri, C., Petrosino, S., Orlando, P., Bentivoglio, M., Mackie, K., and Di Marzo, V. (2013). Obesity-driven synaptic remodeling affects endocannabinoid control of orexinergic neurons. Proc. Natl. Acad. Sci. USA 110, E2229–E2238.

Daumas-Meyer, V., Champeil-Potokar, G., Chaumontet, C., Dahirel, P., Papillon, C., Congar, P., and Denis, I. (2018). Fasting induces astroglial plasticity in the olfactory bulb glomeruli of rats. Glia 66, 762–776.

Dietrich, M.O., and Horvath, T.L. (2013). Hypothalamic control of energy balance: insights into the role of synaptic plasticity. Trends Neurosci. 36, 65–73.

Dodd, G.T., Michael, N.J., Lee-Young, R.S., Mangiafico, S.P., Pryor, J.T., Munder, A.C., Simonds, S.E., Brüning, J.C., Zhang, Z.Y., Cowley, M.A., et al. (2018). Insulin regulates POMC neuronal plasticity to control glucose metabolism. eLife 7.

Durkee, C.A., Covelo, A., Lines, J., Kofuji, P., Aguilar, J., and Araque, A. (2019). G$_{i/o}$ protein-coupled receptors inhibit neurons but activate astrocytes and stimulate gliotransmission. Glia 67, 1076–1093.

Enriori, P.J., Evans, A.E., Sinnayah, P., Jobst, E.E., Tonelli-Lemos, L., Billes, S.K., Glavas, M.M., Grayson, B.E., Perello, M., Nillni, E.A., et al. (2007). Diet-induced obesity causes severe but reversible leptin resistance in arcuate melanocortin neurons. Cell Metab. 5, 181–194.

Farrell, M.S., Pei, Y., Wan, Y., Yadav, P.N., Daigle, T.L., Urban, D.J., Lee, H.M., Sciaky, N., Simmons, A., Nonneman, R.J., et al. (2013). A Gαs DREADD mouse for selective modulation of cAMP production in striatopallidal neurons. Neuropsychopharmacology 38, 854–862.

Fenselau, H., Campbell, J.N., Verstegen, A.M., Madara, J.C., Xu, J., Shah, B.P., Resch, J.M., Yang, Z., Mandelblat-Cerf, Y., Livneh, Y., and Lowell, B.B. (2017). A rapidly acting glutamatergic ARC→PVH satiety circuit postsynaptically regulated by α-MSH. Nat. Neurosci. 20, 42–51.

Fuente-Martín, E., García-Cáceres, C., Granado, M., de Ceballos, M.L., Sánchez-Garrido, M.A., Sarman, B., Liu, Z.W., Dietrich, M.O., Tena-Sempere, M., Argente-Arizón, P., et al. (2012). Leptin regulates glutamate and glucose transporters in hypothalamic astrocytes. J. Clin. Invest. 122, 3900–3913.

Gao, Q., Mezei, G., Nie, Y., Rao, Y., Choi, C.S., Bechmann, I., Leranth, C., Toran-Allerand, D., Priest, C.A., Roberts, J.L., et al. (2007). Anorectic estrogen mimics leptin's effect on the rewiring of melanocortin cells and Stat3 signaling in obese animals. Nat. Med. 13, 89–94.

García-Cáceres, C., Quarta, C., Varela, L., Gao, Y., Gruber, T., Legutko, B., Jastroch, M., Johansson, P., Ninkovic, J., Yi, C.X., et al. (2016). Astrocytic Insulin Signaling Couples Brain Glucose Uptake with Nutrient Availability. Cell 166, 867–880.

García-Cáceres, C., Balland, E., Prevot, V., Luquet, S., Woods, S.C., Koch, M., Horvath, T.L., Yi, C.X., Chowen, J.A., Verkhratsky, A., et al. (2019). Role of astrocytes, microglia, and tanycytes in brain control of systemic metabolism. Nat. Neurosci. 22, 7–14.

Guettier, J.M., Gautam, D., Scarselli, M., Ruiz de Azua, I., Li, J.H., Rosemond, E., Ma, X., Gonzalez, F.J., Armbruster, B.N., Lu, H., et al. (2009). A chemical-genetic approach to study G protein regulation of beta cell function in vivo. Proc. Natl. Acad. Sci. USA 106, 19197–19202.

Gyengesi, E., Liu, Z.W., D'Agostino, G., Gan, G., Horvath, T.L., Gao, X.B., and Diano, S. (2010). Corticosterone regulates synaptic input organization of POMC and NPY/AgRP neurons in adult mice. Endocrinology 151, 5395–5402.

He, Z., Gao, Y., Alhadeff, A.L., Castorena, C.M., Huang, Y., Lieu, L., Afrin, S., Sun, J., Betley, J.N., Guo, H., and Williams, K.W. (2018). Cellular and synaptic reorganization of arcuate NPY/AgRP and POMC neurons after exercise. Mol. Metab. 18, 107–119.

Hoffmann, T.J., Choquet, H., Yin, J., Banda, Y., Kvale, M.N., Glymour, M., Schaefer, C., Risch, N., and Jorgenson, E. (2018). A Large Multi-ethnic Genome-Wide Association Study of Adult Body Mass Index Identifies Novel Loci. Genetics 14, 10.

Horvath, T.L., and Gao, X.B. (2005). Input organization and plasticity of hypocretin neurons: possible clues to obesity's association with insomnia. Cell Metab. 1, 279–286.

Horvath, T.L., Sarman, B., García-Cáceres, C., Enriori, P.J., Sotonyi, P., Shanabrough, M., Borok, E., Argente, J., Chowen, J.A., Perez-Tilve, D., et al. (2010). Synaptic input organization of the melanocortin system predicts diet-induced hypothalamic reactive gliosis and obesity. Proc. Natl. Acad. Sci. USA 107, 14875–14880.

Jones, M.E., Paniccia, J.E., Lebonville, C.L., Reissner, K.J., and Lysle, D.T. (2018). Chemogenetic Manipulation of Dorsal Hippocampal Astrocytes Protects Against the Development of Stress-enhanced Fear Learning. Neuroscience 388, 45–56.

Kim, J.G., Suyama, S., Koch, M., Jin, S., Argente-Arizon, P., Argente, J., Liu, Z.W., Zimmer, M.R., Jeong, J.K., Szigeti-Buck, K., et al. (2014). Leptin signaling in astrocytes regulates hypothalamic neuronal circuits and feeding. Nat. Neurosci. 17, 908–910.

Kong, D., Dagon, Y., Campbell, J.N., Guo, Y., Yang, Z., Yi, X., Aryal, P., Wellenstein, K., Kahn, B.B., Sabatini, B.L., and Lowell, B.B. (2016). A Postsynaptic AMPK→p21-Activated Kinase Pathway Drives Fasting-Induced Synaptic Plasticity in AgRP Neurons. Neuron 91, 25–33.

Krashes, M.J., Koda, S., Ye, C., Rogan, S.C., Adams, A.C., Cusher, D.S., Maratos-Flier, E., Roth, B.L., and Lowell, B.B. (2011). Rapid, reversible activation of AgRP neurons drives feeding behavior in mice. J. Clin. Invest. 121, 1424–1428.

Labouèbe, G., Liu, S., Dias, C., Zou, H., Wong, J.C., Karunakaran, S., Clee, S.M., Phillips, A.G., Boutrel, B., and Borgland, S.L. (2013). Insulin induces long-term depression of ventral tegmental area dopamine neurons via endocannabinoids. Nat. Neurosci. 16, 300–308.

Lam, B.Y.H., Cimino, I., Polex-Wolf, J., Nicole Kohnke, S., Rimmington, D., Iyemere, V., Heeley, N., Cossetti, C., Schulte, R., Saraiva, L.R., et al. (2017). Heterogeneity of hypothalamic pro-opiomelanocortin-expressing neurons revealed by single-cell RNA sequencing. Mol. Metab. 6, 383–392.

Langlet, F., Levin, B.E., Luquet, S., Mazzone, M., Messina, A., Dunn-Meynell, A.A., Balland, E., Lacombe, A., Mazur, D., Carmeliet, P., et al. (2013). Tanycytic VEGF-A boosts blood-hypothalamus barrier plasticity and access of metabolic signals to the arcuate nucleus in response to fasting. Cell Metab. 17, 607–617.

Lim, B.K., Huang, K.W., Grueter, B.A., Rothwell, P.E., and Malenka, R.C. (2012). Anhedonia requires MC4R-mediated synaptic adaptations in nucleus accumbens. Nature 487, 183–189.

Liu, T., Kong, D., Shah, B.P., Ye, C., Koda, S., Saunders, A., Ding, J.B., Yang, Z., Sabatini, B.L., and Lowell, B.B. (2012). Fasting activation of AgRP neurons requires NMDA receptors and involves spinogenesis and increased excitatory tone. Neuron 73, 511–522.

Locke, A.E., Kahali, B., Berndt, S.I., Justice, A.E., Pers, T.H., Day, F.R., Powell, C., Vedantam, S., Buchkovich, M.L., Yang, J., et al.; LifeLines Cohort Study; ADIPOGen Consortium; AGEN-BMI Working Group; CARDIOGRAMplusC4D Consortium; CKDGen Consortium; GLGC; ICBP; MAGIC Investigators; MuTHER Consortium; MIGen Consortium; PAGE Consortium; ReproGen Consortium; GENIE Consortium; International Endogene Consortium (2015). Genetic studies of body mass index yield new insights for obesity biology. Nature *518*, 197–206.

Losciuto, S., Dorban, G., Gabel, S., Gustin, A., Hoenen, C., Grandbarbe, L., Heuschling, P., and Heurtaux, T. (2012). An efficient method to limit microglia-dependent effects in astroglial cultures. J. Neurosci. Methods *207*, 59–71.

Mandelblat-Cerf, Y., Ramesh, R.N., Burgess, C.R., Patella, P., Yang, Z., Lowell, B.B., and Andermann, M.L. (2015). Arcuate hypothalamic AgRP and putative POMC neurons show opposite changes in spiking across multiple timescales. eLife *4*.

Manvich, D.F., Webster, K.A., Foster, S.L., Farrell, M.S., Ritchie, J.C., Porter, J.H., and Weinshenker, D. (2018). The DREADD agonist clozapine N-oxide (CNO) is reverse-metabolized to clozapine and produces clozapine-like interoceptive stimulus effects in rats and mice. Sci. Rep. *8*, 3840.

Melnick, I., Pronchuk, N., Cowley, M.A., Grove, K.L., and Colmers, W.F. (2007). Developmental switch in neuropeptide Y and melanocortin effects in the paraventricular nucleus of the hypothalamus. Neuron *56*, 1103–1115.

Newton, A.J., Hess, S., Paeger, L., Vogt, M.C., Fleming Lascano, J., Nillni, E.A., Brüning, J.C., Kloppenburg, P., and Xu, A.W. (2013). AgRP innervation onto POMC neurons increases with age and is accelerated with chronic high-fat feeding in male mice. Endocrinology *154*, 172–183.

Oliet, S.H. (2002). Functional consequences of morphological neuroglial changes in the magnocellular nuclei of the hypothalamus. J. Neuroendocrinol. *14*, 241–246.

Oliet, S.H., Piet, R., and Poulain, D.A. (2001). Control of glutamate clearance and synaptic efficacy by glial coverage of neurons. Science *292*, 923–926.

Paeger, L., Pippow, A., Hess, S., Paehler, M., Klein, A.C., Husch, A., Pouzat, C., Bruning, J.C., and Kloppenburg, P. (2017). Energy imbalance alters Ca^{2+} handling and excitability of POMC neurons. eLife *6*.

Pinto, S., Roseberry, A.G., Liu, H., Diano, S., Shanabrough, M., Cai, X., Friedman, J.M., and Horvath, T.L. (2004). Rapid rewiring of arcuate nucleus feeding circuits by leptin. Science *304*, 110–115.

Powell, D.R., Smith, M., Greer, J., Harris, A., Zhao, S., DaCosta, C., Mseeh, F., Shadoan, M.K., Sands, A., Zambrowicz, B., and Ding, Z.M. (2013). LX4211 increases serum glucagon-like peptide 1 and peptide YY levels by reducing sodium/glucose cotransporter 1 (SGLT1)-mediated absorption of intestinal glucose. J. Pharmacol. Exp. Ther. *345*, 250–259.

Powell, D.R., DaCosta, C.M., Smith, M., Doree, D., Harris, A., Buhring, L., Heydorn, W., Nouraldeen, A., Xiong, W., Yalamanchili, P., et al. (2014). Effect of LX4211 on glucose homeostasis and body composition in preclinical models. J. Pharmacol. Exp. Ther. *350*, 232–242.

Rathjen, T., Yan, X., Kononenko, N.L., Ku, M.C., Song, K., Ferrarese, L., Tarallo, V., Puchkov, D., Kochlamazashvili, G., Brachs, S., et al. (2017). Regulation of body weight and energy homeostasis by neuronal cell adhesion molecule 1. Nat. Neurosci. *20*, 1096–1103.

Richard, C.D., Tolle, V., and Low, M.J. (2011). Meal pattern analysis in neural-specific proopiomelanocortin-deficient mice. Eur. J. Pharmacol. *660*, 131–138.

Roth, B.L. (2016). DREADDs for Neuroscientists. Neuron *89*, 683–694.

Scofield, M.D., Boger, H.A., Smith, R.J., Li, H., Haydon, P.G., and Kalivas, P.W. (2015). Gq-DREADD Selectively Initiates Glial Glutamate Release and Inhibits Cue-induced Cocaine Seeking. Biol. Psychiatry *78*, 441–451.

Sohn, J.W., and Williams, K.W. (2012). Functional heterogeneity of arcuate nucleus pro-opiomelanocortin neurons: implications for diverging melanocortin pathways. Mol. Neurobiol. *45*, 225–233.

Su, Z., Alhadeff, A.L., and Betley, J.N. (2017). Nutritive, Post-ingestive Signals Are the Primary Regulators of AgRP Neuron Activity. Cell Rep. *21*, 2724–2736.

Suyama, S., Ralevski, A., Liu, Z.W., Dietrich, M.O., Yada, T., Simonds, S.E., Cowley, M.A., Gao, X.B., Diano, S., and Horvath, T.L. (2017). Plasticity of calcium-permeable AMPA glutamate receptors in Pro-opiomelanocortin neurons. eLife *6*.

Sweeney, P., Qi, Y., Xu, Z., and Yang, Y. (2016). Activation of hypothalamic astrocytes suppresses feeding without altering emotional states. Glia *64*, 2263–2273.

Theodosis, D.T., Poulain, D.A., and Oliet, S.H. (2008). Activity-dependent structural and functional plasticity of astrocyte-neuron interactions. Physiol. Rev. *88*, 983–1008.

Vardjan, N., Kreft, M., and Zorec, R. (2014). Dynamics of β-adrenergic/cAMP signaling and morphological changes in cultured astrocytes. Glia *62*, 566–579.

Vong, L., Ye, C., Yang, Z., Choi, B., Chua, S., Jr., and Lowell, B.B. (2011). Leptin action on GABAergic neurons prevents obesity and reduces inhibitory tone to POMC neurons. Neuron *71*, 142–154.

Walsh, R.N., and Cummins, R.A. (1976). The Open-Field Test: a critical review. Psychol. Bull. *83*, 482–504.

Wang, M., Wang, Q., and Whim, M.D. (2016). Fasting induces a form of autonomic synaptic plasticity that prevents hypoglycemia. Proc. Natl. Acad. Sci. USA *113*, E3029–E3038.

Willer, C.J., Speliotes, E.K., Loos, R.J., Li, S., Lindgren, C.M., Heid, I.M., Berndt, S.I., Elliott, A.L., Jackson, A.U., Lamina, C., et al.; Wellcome Trust Case Control Consortium; Genetic Investigation of ANthropometric Traits Consortium (2009). Six new loci associated with body mass index highlight a neuronal influence on body weight regulation. Nat. Genet. *41*, 25–34.

Williams, K.W., Margatho, L.O., Lee, C.E., Choi, M., Lee, S., Scott, M.M., Elias, C.F., and Elmquist, J.K. (2010). Segregation of acute leptin and insulin effects in distinct populations of arcuate proopiomelanocortin neurons. J. Neurosci. *30*, 2472–2479.

Yang, Y., Atasoy, D., Su, H.H., and Sternson, S.M. (2011). Hunger states switch a flip-flop memory circuit via a synaptic AMPK-dependent positive feedback loop. Cell *146*, 992–1003.

Yang, S.B., Tien, A.C., Boddupalli, G., Xu, A.W., Jan, Y.N., and Jan, L.Y. (2012). Rapamycin ameliorates age-dependent obesity associated with increased mTOR signaling in hypothalamic POMC neurons. Neuron *75*, 425–436.

Yang, L., Qi, Y., and Yang, Y. (2015). Astrocytes control food intake by inhibiting AGRP neuron activity via adenosine A1 receptors. Cell Rep. *11*, 798–807.

Zeltser, L.M., Seeley, R.J., and Tschöp, M.H. (2012). Synaptic plasticity in neuronal circuits regulating energy balance. Nat. Neurosci. *15*, 1336–1342.

Zhan, C., Zhou, J., Feng, Q., Zhang, J.E., Lin, S., Bao, J., Wu, P., and Luo, M. (2013). Acute and long-term suppression of feeding behavior by POMC neurons in the brainstem and hypothalamus, respectively. J. Neurosci. *33*, 3624–3632.

STAR★METHODS

KEY RESOURCES TABLE

REAGENT or RESOURCE	SOURCE	IDENTIFIER
Antibodies		
Rabbit polyclonal anti-DsRed	Ozyme	Cat# 632496; RRID:AB_10013483
Biotinylated goat polyclonal anti-rabbit IgG	Vector Laboratories	Cat# BA-1000; RRID:AB_2313606
Guinea pig polyclonal anti-VGluT1	Synaptic Systems	Cat# 135 304; RRID:AB_887878
Mouse monoclonal anti-VGAT	Synaptic Systems	Cat# 131 011; RRID:AB_887872
Alexa Fluor 594-conjugated anti-rabbit	ThermoFisher Scientific	Cat# A-21207; RRID:AB_141637
Alexa Fluor 633-conjugated goat anti-guinea pig	ThermoFisher Scientific	Cat# A-21105; RRID:AB_2535757
Alexa Fluor 488-conjugated goat anti-mouse	ThermoFisher Scientific	Cat# A-11001; RRID:AB_2534069
Mouse monoclonal anti-GFP	Roche	Cat# 11814460001; RRID:AB_390913
Anti-GFAP	Dako	Cat# Z0334; RRID:AB_10013382
Anti-mouse CD11b antibody-conjugated MicroBeads	Miltenyi Biotec	Cat# 130-093-636; RRID:AB_2783886
Bacterial and Virus Strains		
AAV8/GFAP-HA-hM4G(Gi)-mCitrine	Translational Vector Core	N/A
Chemicals, Peptides, and Recombinant Proteins		
LX4211	Advanced Chemblocks	G-5684
CNO	Enzo Life Sciences	BML-NS105-0005
Tetrodotoxin, TTX	Tocris	1069
Picrotoxin	Sigma-Aldrich	P1675
Cesium chloride, CsCl	Sigma-Aldrich	289329
Potassium gluconate, K-Glu	Sigma-Aldrich	G4500
Diaminobenzidine	Vector Laboratories	SK4100
Forskolin	Sigma-Aldrich	F6886
Critical Commercial Assays		
AlphaLISA Insulin immunoassay kit	Perkin Elmer	AL204C
Leptin Quantikine ELISA kit	R&D Systems	MOB00
Acylated Ghrelin Express EIA kit	Bertin Pharma	A05117
Vectastain ABC Elite (HRP) kit	Vector laboratories	PK6100
Cytotoxicity Detection Kit (LDH)	Roche Applied Science	11644793001
cAMP-GloTM Max Assay	Promega	V1681
Experimental Models: Organisms/Strains		
Pomc^{Cre}	Jackson Laboratories	Stock No. 005965
tdTomato^{flox/flox}	Jackson Laboratories	Stock No. 007914
C57/BL6	Charles River	632C57BL/6J
Software and Algorithms		
Prism 5.0	GraphPad Software	N/A
Imaris	Bitplane	N/A
Other		
Standard diet	Safe	A04
High fat diet	Safe	U8954 v7
High sucrose diet	Safe	AIN76A

LEAD CONTACT AND MATERIALS AVAILABILITY

Further information and requests for resources and reagents should be directed to and will be fulfilled by the Lead Contact, Alexandre Benani (alexandre.benani@u-bourgogne.fr). This study did not generate new unique reagents.

EXPERIMENTAL MODEL AND SUBJECT DETAILS

Mice

Transgenic *POMC*[Cre:tdTomato] mice were obtained by crossing *Pomc*[Cre] (Stock No. 005965) with *tdTomato*[flox/flox] (Stock No. 007914) mice, which were purchased from Jackson Laboratories. Experiments were made on 7/10-week old male that were heterozygous for *POMC* (cre+/−) and homozygous for *tdTomato*. Animals were housed at $22.5 \pm 1°C$ on a 12h-12h reversed light-dark cycle (light off at 10h30; light on at 22h30). Before experiments, animals had free access to standard diet (A04, SAFE) and water. Telemetry studies were performed on male mice C57BL/6J from Charles River. These mice were housed individually in a room maintained at $22.5 \pm 1°C$ with light from 7:00 am to 7:00 pm. Food (#A04; Safe) and water were given *ad libitum*. Mice were kept individually for at least 7 days in their own cages before surgical procedure. All protocols including animals were reviewed by our local ethic committee in strict accordance with European Community guidelines and agreed by the French Ministry of Higher Education and Research (accreditation No. 00853.01).

Experimental design

Three groups of mice were designed to compare prandial states (Figure S1A). For experiments, mice were submitted to a 2-hour food restriction just before lights off. This procedure was designed to standardize the metabolic state of mice and minimize variation in their sensation of hunger. This also ensures substantial and reliable food intake after food reintroduction. This physiological "no food condition" does not alter level of metabolic hormones. Preprandial mice (Pre) were killed just after food restriction. Postprandial mice received food at lights off for 1 hour and were killed after the feeding period. Food was either a standard diet (SD; Cat. No. A04; Safe), a high-fat diet (HFD; semi-synthesized diet, Cat. No. U8954 v7; Safe) or a high-sucrose low-fat diet (HSD; Cat. No. AIN76A; Safe). Diet compositions are given in the Table S1.

Before experiments, mice were housed individually for 3 days in their regular cages and were trained for the 2-hour food restriction. To prevent food neophobia, mice received some HFD pellets for 10 minutes 1 day before the experiment. An additional group of fasted mice was generated as a reference. These mice were killed after 24-hour fast. In graphs, preprandial mice were noted: "Pre-prandial," while mice receiving standard and HFD for 1 hour were noted: "1h-SD" and "1h-HFD," respectively.

Primary astrocyte culture

Primary glial cell cultures were prepared from newborn C57BL/6J mouse brains (Harlan) as described elsewhere (Losciuto et al., 2012). Sex of newborn mice was not determined. Microglial cells were removed from the cultures using a magnetic separation kit (Miltenyi Biotec) according to the manufacturer's instructions. Precisely, confluent cultures were washed with PBS, trypsinized and centrifuged. Cell pellet was resuspended in a rinsing solution (AutoMACS Rinsing Solution, Miltenyi Biotec) and was further centrifuged at 300 g at $4°C$ for 10 min. Cells were resuspended in the rinsing solution (1×10^7 cells in 90 µl), mixed with 10 µl of monoclonal rat anti-mouse CD11b antibody-conjugated MicroBeads (Miltenyi Biotec), and incubated at $4°C$ for 20 min with gentle mixing after 10 min. Then, cells were washed with the rinsing solution and centrifuged at 300 g at $4°C$ for 10 min. Cells were resuspended in the rinsing solution (500 µL for 1×10^8 cells) and transferred in a LS column (Miltenyi Biotec) fixed to MidiMACS magnetic separation unit (Miltenyi Biotec), after prior washing of the column with the rinsing solution (3x3 ml). Unbound cells corresponding to astrocytes, were eluted from the column, centrifuged at 300 g at $4°C$ for 10 min, and resuspended in complete medium before plating. In order to vastly reduce microglial contamination, a second magnetic cell sorting (as done before) was performed after 6-7 days, to obtain pure astrocyte cultures with less than 0.5% microglia and virtually no others brain cells. Astrocytes were then cultured for 1 week. At 70% confluence, the medium was renewed and astrocytes were transduced with 3×10^9 vg/ml AAV8/GFAP-HA-hM4G(Gi)-mCitrine (Translational Vector Core, Nantes, France). After 48 h, astrocytes were treated with 10 µM Forskolin (Sigma) and/or 10 µM CNO (Sigma) for 20 minutes before viability assay or cAMP assay.

METHOD DETAILS

Stereotactic injections

Mice were anesthetized by ip injection of a ketamine-xylazine mix (80mg/kg - 12 mg/kg). They were then placed on a stereotaxic frame. AAV8/GFAP-HA-hM4G(Gi)-mCitrine (Translational Vector Core, Nantes, France) virus were injected bilaterally into the arcuate nucleus of the hypothalamus. Stereotactic co-ordinates relative to bregma were: x: ± 0.3 mm; y: +1.5 mm; z: −6 mm. Injection were done at a rate of 0.5 µl/min for 1 min per side. At the end of surgical procedures, mice received 1 mg/kg i.p. atipamezole and 5 mg/kg s.c. ketoprofen.

Drug administration

Glucose was prepared in water and injected at 0.5 g/kg (ip, 100 µl), 30-45 minutes before lights off. LX4211 (Sotagliflozin; dual SGLT1/ SGLT2 inhibitor) was purchased from Advanced Chemblocks. LX4211 was prepared in NaCl 0.9% containing 2.5% DMSO, 22.5% PEG300. LX4211 was injected at 10 mg/kg (ip, 100 µl), 30-60 minutes before lights off. CNO was purchased from ENZO Life Sciences. CNO was prepared in water at a stock concentration of 5 mg/mL (20X) and stored at −80°C. CNO working solutions

were diluted in water. CNO was injected at 1 mg/kg (ip, 100 μl), 30-45 minutes before lights off. Before all experiments, mice were trained 3 times with i.p. injections of saline once a day, before light off.

Blood biochemistry
Blood samples were collected in awake animals at the tail tip after incision. Plasmas were obtained by centrifugation at 2650 *g* for 10 min at 7°C. For acyl ghrelin determination, blood samples were collected on EDTA (1 mg/mL final) and p-Hydroxy-mercuribenzoic acid (0.4 mM final), a serine protease inhibitor. After centrifugation plasma was acidified with HCl (0.1 N final) to preserve acylation. Aliquots were stored at −80°C until use. Plasma insulin was measured using the bead-based AlphaLISA Insulin immunoassay kit (Cat. No. AL204C; Perkin Elmer). Plasma leptin was measured using the Leptin Quantikine ELISA kit (Cat. No. MOB00; R&D Systems). Acylated ghrelin was measured using the Acylated Ghrelin Express EIA Kit (Cat. No. A05117; Bertin Pharma).

Continuous monitoring of feeding behavior
Food intake was recorded in undisturbed mice using the automated BioDAQ System (Research Diets, Inc.). Mice were habituated for one week to single housing in a regular cage and feeding through a food hopper. Cages contained enrichment and bedding material. Water was given *ad libitum* from regular bottles placed on the top of the cage. Mice showed normal food intake and body weight gain within 3 days of habituation. During habituation and experiments, food hoppers were closed for 2 hours before light off. Data were collected continuously during experiments and were analyzed using the BioDAQ DataViewer software (Research Diets, Inc.). For analysis, the minimum food amount was filtered at 0.02 g and the minimum inter-bout interval, which separates two feeding bouts, was defined as 5 s. For pharmacogenetics studies, mice were randomly assigned to receive a single injection of CNO or NaCl per day. Treatment and vehicle were injected alternatively in the same mice, allowing paired analyses.

Continuous monitoring of glycemia
Telemetric devices (Data Sciences International) were implanted according to the manufacturer instructions. Briefly, mice were anesthetized with isoflurane and received ip injection of 10 mg/kg buprenorphine (Buprecare® 0.3 mg/ml) and 10 mg/kg ketoprofen (Ketofen® 10%). The sensor (HD-XG; Data Sciences International) was placed into the left carotid toward the aortic arch. After surgery, animals were allowed to recover at 35°C and received a daily ip injection of ketoprofen (Ketofen® 10%) for 3 days. During a 7-day recovery period, individualized mice were carefully monitored for body weight and behavior and had facilitated access to food. Implanted animals were then installed on their own receiver. An initial calibration was accomplished through an oral glucose tolerance test (2 g/kg of 30% glucose). Blood was sampled from the tail vein at two times points (before gavage and at 3 min after glucose load) in order to assay glucose concentration with a glucometer. Data was collected using the Ponemah® software (DSI).

Open Field Test
An open field test was used to assess locomotor activity and anxiety-like behavior in mice. The open field consisted of a plexiglas chamber (43.5 cm x 43.5 cm x 30.5 cm) placed inside a frame containing infrared photobeams sources and sensors, which detect the presence of animal in a spatial and temporal manner along the three axis (x, y, z) (Activity Monitor system; Med Associates, Inc.). Animal activity was monitored and analyzed with the Activity Monitor software (Med Associates, Inc.). For analysis, arena was divided into two zones: center and periphery. For trial, food was removed 2 hours at the end of the light period, as indicated before. Mice received a single injection of either NaCl or CNO solution intraperitoneally, one hour before light off. At light off, animals were fed for 3 hours using standard diet and then placed into the arena, in a randomized corner. Behavior was recorded during 30 minutes. Between each trial, arena was cleaned and dried. Numbers of entries in the center, percentage of time spent in the center compared to the periphery and total ambulatory distance were measured.

Electrophysiology
Experiments were performed on brain slices from 7/9-week old mice. Animals were anesthetized with a ketamine/xylazine mix (80 mg/kg - 8 mg/kg) and transcardially perfused with an ice-cold and oxygenated (95% O_2 / 5% CO_2) Slicing Solution (SS; 20 ml) which contains (in mM): 200 sucrose, 28 $NaHCO_3$, 2.5 KCl, 7 $MgCl_2$, 1.25 NaH_2PO_4, 0.5 $CaCl_2$, 5 HEPES, 1 ascorbate; 8 D-glucose; 3 Na-pyruvate (pH = 7.25-7.30, adjusted with HCl 5N). After perfusion, brains were rapidly extracted and placed on the stage of a thermostated vibrating microtome (Vibroslice, Leica VT1000S). Frontal brain sections containing the arcuate nucleus of the hypothalamus (250 μm thick) were cut at 4°C in the oxygenated SS. Slices were then incubated in an oxygenated bath of 5 mM glucose Extracellular Solution (5G-ES), which contains (in mM): 118 NaCl, 3 KCl, 1.2 NaH_2PO_4, 1 $MgCl_2$, 25 $NaHCO_3$, 1.5 $CaCl_2$, 5 HEPES, 5 glucose (pH = 7.3-7.4, adjusted with HCl 5N; osmolarity = 300-310 mOsmol/L, adjusted with sucrose), for 30 min at room temperature. Slices were further incubated in an oxygenated bath of 2.5 mM glucose Extracellular Solution (2.5G-ES) for 1 hour at least, at room temperature, until ready to record. For recording, slices were placed into a chamber (RC-40LP; Warner Instruments) and perfused with 2.5G-ES (flow rate = 3 ml/min. Cells were visualized using a microscope (BX-RFA; Olympus) equipped with a 60X water-immersion objective (LUMPlanFLN; Olympus) and an IR-DIC-sensitive camera (Rolera Bolt; QImaging). Fluorescent cells were identified using a fluorescent lamp (X-Cite 120Q; Excelitas) with an excitation filter for tdTomato protein (mCherry HC Filter Set, Cat. No. F36-508; AHF). Microscope images were acquired and enhanced with QCapture Pro software (QImaging). Electrodes were made from borosilicate glass capillaries (outer diameter: 1.5 mm; inner diameter: 0.86 mm; length: 10 cm; Sutter Instruments) with a

pipette-puller (Model P-1000; Sutter Instruments). Only electrodes with a resistance between 5 to 7 MΩ were used. Small positive pressure was applied to electrodes before their insertion into the slices with a micromanipulator (MP225; Sutter Instruments).

For recording of spontaneous cell firing activity in cell-attached configuration, electrodes were filled with 2.5G-ES. For recording of mEPSC in whole-cell configuration (voltage-clamp −65 mV), electrodes were filled with a K-gluconate Intracellular Solution (KGlu-IS), which contains (in mM): 138 K-gluconate, 4 Na-gluconate, 4 MgCl$_2$, 10 HEPES, 5 EGTA, 2 Na$_2$-ATP, 0.4 Na$_2$-GTP (E_{K+} = −100.7 mV; E_{Cl^-} = −72.0 mV; pH = 7.2-7.3, adjusted with KOH 1N; osmolarity 290 mOsmol/L, adjusted with sucrose) in presence of picrotoxin (25 μM) and tetrodotoxin (TTX; 500 nM). For recording of mIPSC in whole-cell configuration (voltage-clamp −65 mV), electrodes were filled with a cesium-chlorure Intracellular Solution (Cs-IS), which contain (in mM) 140 CsCl; 3.6 NaCl, 1 MgCl$_2$, 10 HEPES; 0.1 Na$_4$-EGTA, 2 Na$_2$-ATP, 0.4 Na$_2$-GTP; (E_{K+} = - ∞ ; E_{Cl^-} = 3.68 mV; osmolarity = 280 mOsmol/L, adjusted with sucrose; pH = 7.2-7.3 adjusted with NaOH 1N) in presence of TTX (500 nM).

Electrical activities were recorded with an amplifier (EPC10; Heka Elektronik) connected to an acquisition interface (LIH 8+8; Heka Elektronik). Acquisitions were done with Patchmaster software (Heka Elektronik) and data were analyzed with Clampfit software (10.3.0.2, Molecular Device Inc.). For cell-attached recordings, neuronal activities were recorded during 10 minutes, after 3 to 5 minutes of stabilization post-sealing. Analysis was done on the last 2 minutes of recording. For whole-cell recordings of miniature postsynaptic currents, the amplifier filter was adjusted to 2 kHz. For mEPSC, picrotoxin was applied for 6 minutes, and then TTX was applied for 10 minutes. For mIPSC, TTX was equally applied for 10 minutes. Neuronal activities were recorded for 10 minutes and analyses were done over the last 3 minutes of recording.

Electrophysiological recordings were performed on 2-3 arcuate nucleus-containing brain slices per day collected from one mouse. Slice preparation lasted 40 minutes, and each slice was then recorded during 1 hour after a minimal 1h-recovery (Table S3).

Electron microscopy

Animals were anesthetized by ip injection of a ketamine-xylazine mix (80mg/kg - 12 mg/kg) and perfused intracardiacally with PBS (15 ml) and with 4% paraformaldehyde - 0.5% glutaraldehyde prepared in 0.1M PB (40 ml). Brains were removed and postfixed overnight at 4°C in the fixative solution. Brains were then cut in 50-μm thick frontal sections using a vibratome (VT 1200S, Leica) and sections containing the arcuate nucleus were collected. Immunohistochemistry against Tomato was performed. Briefly, free-floating sections were first treated in the dark with H$_2$O$_2$ diluted in PBS (0.1%, 15 min) at room temperature, and incubated for 2 hours at room temperature in a blocking solution containing 1% BSA, 1% NGS, 0.01% saponin in PBS. Sections were then incubated overnight at 4°C with primary antibody against tdTomato diluted in the blocking solution containing saponin (1/2500, rabbit polyclonal anti-DsRed; Ozyme). After washing in PBS (3x20 min), sections were incubated for 2 hours at room temperature with the secondary antibody diluted in the blocking solution containing saponin (1/800, biotinylated goat polyclonal anti-rabbit IgG; #BA-1000, Vector Laboratories). After washing in PBS (3x20 min), immune complexes were amplified using the avidin-biotin enzyme system (Vectastain ABC Elite (HRP) kit, #PK6100; Vector laboratories), for 1h at room temperature. Immune complexes were detected with diaminobenzidine (Vector DAB Kit, #SK4100; Vector Laboratories), for 8 min at room temperature. After this immunodetection step, sections were further fixed in 1% glutaraldehyde prepared in 0.1M PB for 1 hour, and rinced in PBS (3x10 min). Sections were osmified with 0.4% OsO4 in PBS for 2 hours at room temperature, and rinsed in PBS (3x10 min). Then sections were rapidly dehydrated and then embedded in epoxy resin (Durcupan, Sigma) between Aclar embedding films (Ted Pella Inc.). 80-nm ultrathin sections were cut with an ultramicrotome and collected on copper-palladium 300 mesh grids (#AGG2300PD; Agar scientific). Sections were contrasted with uranyl-less and lead citrate (Delta Microscopies) before observation. Ultrathin immunostained sections were examined with a transmission electron microscope (7500, Hitachi) and digital images were acquired using CCD camera (AMT) and software (AMT). tdTomato-positive neurons were identified via dark DAB-related signal at x 6,000-8,000 magnification. Morphometric analyses were performed on digitalized images acquired at x 30,000 magnification, taken around one tdTomato-positive neuron. Only neurons for which nuclei were visible were taken into consideration for analysis.

Confocal microscopy

For synaptic puncta analysis, mice were anaesthetized by ip injection of a ketamine/xylazine mix (80 mg/kg - 12 mg/kg) and perfused intracardiacally with PBS (15 ml) and 4% paraformaldehyde prepared in 0.1M PB (40 ml). Brains were removed and postfixed overnight at 4°C in the 4% paraformaldehyde solution. Brains were cryoprotected in 30% sucrose prepared in 0.1 M PB, during 3 days at 4°C. They were then frozen in isopentane at −65°C, and finally stored at −80°C until use. Brains were cut into 16-μm thick frontal sections with a cryostat (CM 3050S, Leica), and serial sections including the arcuate nucleus were collected on SuperFrost Ultra Plus slides (Thermo Scientific). Sections were then processed for immunohistochemistry. Briefly, sections were blocked for 2 hours at room temperature in a blocking solution (NGS 1%, BSA 1%, Triton 0.3%, in PBS), and then incubated overnight at 4°C with a primary antibody prepared in the blocking solution. Primary antibodies were diluted as follows: rabbit polyclonal anti-DsRed (ClonTech), 1/2500; guinea pig polyclonal anti-VGluT1 (Synaptic Systems), 1/2000; mouse monoclonal anti-VGAT (Synaptic Systems), 1/300. After washing in PBS (3x15 min), sections were incubated with secondary antibodies diluted in the blocking solution (1/1000), for 2 hr at room temperature. Secondary antibodies were goat Alexa Fluor 594-conjugated anti-rabbit, Alexa Fluor 633-conjugated goat anti-guinea pig, and Alexa Fluor 488-conjugated goat anti-mouse, (Life Technologies). After further washes in PBS (3x5 min), sections were finally held with mounting medium (Fluoromount, Dako) and coverslip. Acquisitions were done with a confocal laser-scanning microscope (SP2, Leica) using a X63 oil-immersion objective. Z stack acquisition was done with 0.5 μm interval.

For assessment of viral transduction in astrocytes, 30 μm thick fixed brain coronal sections were cut on a vibratome, blocked for 1h with 5% BSA in PBS containing 0.1%Triton X-100 and incubated with primary antibodies overnight at 4°C. Primary antibodies were against GFP (1:000; #11814460001, Roche) and GFAP (1:300; #Z0334, Dako). Adequate AlexaFluor conjugated secondary antibodies were used for immunofluorescence microscopy. Sections were mounted in Vectashield solution (H-1000, Vector Laboratories). Images were acquired with confocal laser-scanning microscope (Leica TCS SP5).

Image analysis

All image analyses were carried out blindly, i.e., without disclosing the experimental group of mice, by one experimenter. For electron microscopy analysis, one ultrathin section per embedded block was observed to avoid counting the same neuron, and 1-3 blocks have been used per animal. Synaptic and glial elements were identified on printed images, which were acquired at an original x 30,000 magnification, according to standard morphological criteria. Synapses were detected as small and round objects around somas, enriched in mitochondria and vesicles, and presenting electron-dense pre- and post-synaptic structures. Glia was defined as light filament around somas, with cloudy glycogen-related granulation. Number of synapses and glial elements was counted directly on printed images. Morphometric study for determination of neuronal perimeter and glial coverage was computed with the open source ImageJ software on digitalized images acquired at x 6,000-8,000 original magnification.

For synaptic puncta analysis, microphotographs from confocal microscopy were analyzed with Imaris software (Bitplane). Surface rendering was done for each channel prior to contact analysis. Contacts between pre-synaptic puncta and POMC neurons were determined using the "Surface Surface Contact Area" plug-in (Imaris, Bitplane). To assess somatic puncta, numbers of contacts between VGAT-positive elements and VGluT1-positive elements were counted on a single tdTomato-positive soma. To assess peri-somatic puncta, contacts between synaptic puncta and tdTomato-positive fibers were determined on 3 regions of interest (ROI) per image. Each standardized ROI (300 μm^2) were designated to exclude tdTomato-positive soma. In these ROIs, contacts between tdTomato-positive objects and VGAT-positive elements or VGluT1-positive elements were counted. Scores were standardized by calculating the ratio between VGluT1-positive elements and VGAT-positive elements per soma or per ROI.

Cytotoxicity assay in primary astrocyte culture

Toxicity of treatments in primary astrocyte cultures were checked with a cytotoxicity detection kit (Roche Applied Science) based on the measurement of LDH activity released from damaged cells. According to the manufacturer's instructions, a fraction of the culture supernatants was used after treatments and incubated for up to 30 min at room temperature with a freshly prepared reaction mixture (v/v). Absorbance was determined at 490 nm using a microplate reader (Tecan). Viability was estimated from the absorbance of treated versus untreated cells (100%).

cAMP assay in primary astrocyte culture

Intracellular levels of 3′,5′-cyclic adenosine monophosphate (cAMP) was measured after treatments in primary astrocyte cultures using the luminescence-based cAMP-GloTM Max Assay (Promega). According to the manufacturer's protocol, intracellular cAMP levels were measured and quantified using a cAMP standard curve. Luminescence was measured using a microplate reader (FLUOstar OPTIMA, BMG Labtech).

QUANTIFICATION AND STATISTICAL ANALYSIS

Statistical analyses were performed using Prism 5.0 software (GraphPad Software, Inc.). No statistical method was used to predefine sample size. Results on graphs were expressed as means and error bars indicated standard errors of the mean (SEM). Comparisons between 2 groups were carried out using two-tailed Student test or nonparametric Mann-Whitney test, as appropriate. Multiple comparisons of groups were carried out using one-way analysis of variance (ANOVA) followed by post hoc Newman-Keuls test or using nonparametric Kruskal-Wallis test followed by post hoc Dunns test, as appropriate. Equality of variances and normality of distribution were checked prior each analysis. No correction was applied on data for analyses. A p value < 0.05 was considered statistically significant. Significant difference was noted *, **, or *** on the graphic representation when p value was < 0.05, 0.01, and 0.001, respectively.

DATA AND CODE AVAILABILITY

This study did not generate any unique datasets or code.